Electronic Supplementary Material (ESI) for ChemComm.

Assessment of encapsulated dyes' distribution in silica nanoparticles and their ability to release useful singlet oxygen.

Vladimir Kabanov, David J Press, Racheal PS Huynh, George KH Shimizu and Belinda Heyne*

University of Calgary, Department of Chemistry,

2500 University Drive NW, Calgary, Alberta, Canada, T2N 1N4

*Email: bjmheyne@ucalgary.ca

Table of Contents:

1. Synthetic Procedures

Chemicals: All reagents were purchased from Sigma-Aldrich and used without further purification unless otherwise stated.

1.1 Synthesis of BODIPY photosensitizer.

Scheme 1 was followed to obtain BODIPY (BDP/BDP-3) photosensitizer, each synthetic step is detailed below. All ^{1}HNMR and ^{13}CNMR were obtained using Bruker Avance 400MHz nuclear magnetic resonance spectrometer. Residual solvent peaks for chloroform-d ($CDCl_3$: ^{1}HNMR (400MHz) δ=7.26 ppm, ^{13}CNMR 100Mhz) δ=77.2 ppm) and methanol-d_4 (MeOD: ^{1}HNMR (400MHz) δ=3.31 ppm, ^{13}CNMR (100Mhz) δ=49.0 ppm) were used as a reference.[1] Mass spectrometry analysis was carried out via electrospray ionization (ESI) methodology on an Agilent Q-TOF 6520 high resolution mass spectrometer.

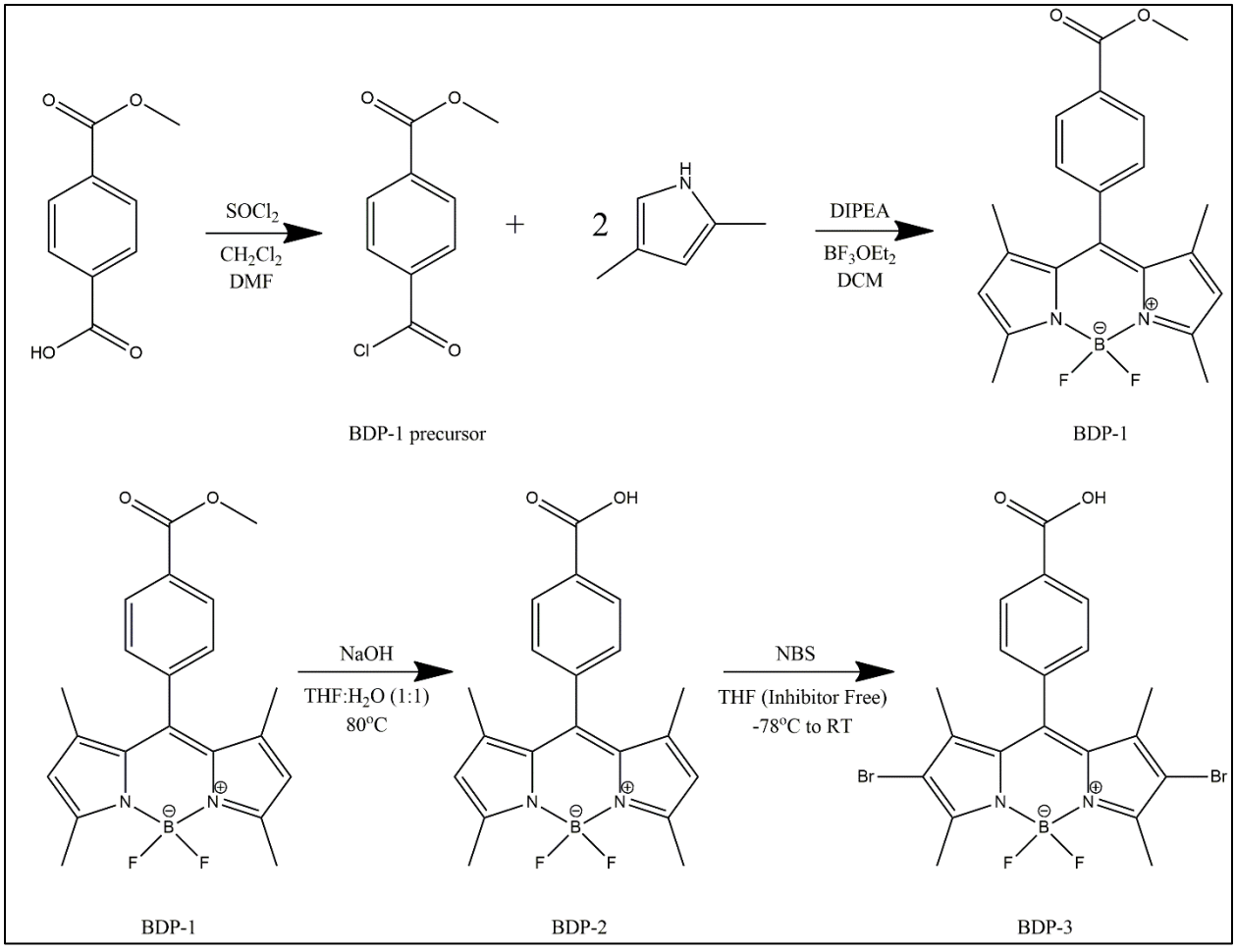

Scheme S1: Synthetic strategy to obtain BODIPY photosensitizer (referred to as BDP in the main text).

Synthesis of methyl 4-(chlorocarbonyl)benzoate (BDP-1 precursor): 2.511 g (13.96 mmol) of mono-methyl terephthalate was suspended in 25 mL of chloroform while under argon. Addition of 10 drops of DMF and 6.0 mL (84 mmol) of thionyl chloride followed. Solution was brought up to 80 °C and left to reflux while stirring under inert atmosphere for 4 hours. Upon reaction completion, solvents from the mixture containing the product (methyl 4-(chlorocarbonyl)benzoate) were evaporated yielding a white powder material which was used immediately without further purification.

Synthesis of the BDP-1: The synthesis was performed based on a modified procedure from Krumova and Cosa (2010).[2] Crude methyl 3-(chlorocarbonyl) benzoate (BDP-1 precursor) from above was dissolved in 175 mL of dried DCM. Under argon, 3.0 mL (28 mmol) of 2,4-dimethyl pyrrole were added and mixture was left to reflux at 50 °C for 2 hours. Upon completion, the contents were cooled to room temperature and 10 mL (57 mmol) of N,N-diisopropylethylamine (DIPEA) were added. The mixture was left to stir for 15 min under argon, followed by addition of 7.0 mL (57 mmol) of boron trifluoride diethyl etharate (BF_3OEt_3). After 15 minutes the reaction mixture was opened to air and was quenched by adding an excess amount of water (appx. 150 mL). The mixture was transferred into a separatory funnel and the crude product was extracted into ethyl acetate. The organic phase was separated, dried ($MgSO_4$) and concentrated. Crude product was purified via flash column chromatography (silica, $CHCl_3$) and 1.14 g (2.97 mmol; 21.3% yield) of red-orange crystalline product BDP-1 was collected and characterized. ^{1}HNMR δ (400 MHz, $CDCl_3$): 1.34 (6H, s, CH_3), 2.54 (6H, s, CH_3), 3.95 (3H, s, CH_3), 5.97 (2H, s, CH), 7.37 (2H, d, J = 8 Hz, phenyl), 8.16 (2H, d, J = 8 Hz, phenyl); figure S1. ^{13}CNMR δ (100 MHz, $CDCl_3$): 14.7, 52.5, 121.6, 121.7, 128.5, 130.5, 131.0, 131.1, 140.0, 140.4, 143.0, 156.2 166.6; figure S2. HRMS(ESI) *m/z*: calc. for $C_{21}H_{22}BF_2N_2O_2^+$ $[M+H]^+$: 383.1742, found: 383.1741.

Synthesis of the BDP-2: Based on modified procedure from Hong *et al.* (2012).[3] Saponification of 230 mg (0.603 mmol) BDP-1 was set up in 30 mL of ACS grade THF, to which 120 mg (2.05 mmol) of NaOH dissolved in 30 mL of water was added. This mixture was refluxed for 5 hours at 80 °C. Upon completion, the mixture was acidified using 1M HCl to a pH of 2 and the crude product was extracted into ethyl acetate, which was dried ($MgSO_4$), filtered and concentrated under reduced pressure. Purification was performed via flash column (silica, 9:1 ethyl acetate:methanol) to yield 73 mg (0.20 mmol, 26.3% yield) of orange crystalline product BDP-2. ^{1}HNMR δ (400 MHz, MeOD): 1.39 (6H, s, CH_3), 2.55 (6H, s, CH_3), 6.05 (2H, s, CH), 7.47 (2H, d, J = 8 Hz, phenyl), 8.20 (2H, d, J = 8 Hz, phenyl); figure S3. ^{13}CNMR δ (100 MHz, MeOD): 14.7, 15.0, 122.5, 129.7, 130.0, 131.7, 132.2, 132.8, 141.4, 142.0, 143.4, 157.1, 169.1; figure S4. HRMS(ESI) *m/z*: calc. for $C_{20}H_{16}BF_2N_2O_2^+$ $[M-3H]^+$: 365.1273, found: 365.1481.

Synthesis of the BDP-3 (BDP): Based on a modified procedure from Goswami *et al.* (2015).[4] 70 mg (0.19 mmol) of BDP-2 was dissolved in 3 mL of dry THF and cooled to -78 °C. While stirring, 141 mg (0.792 mmol) N-bromosuccinimide (NBS) in 2 mL of dry, inhibitor free THF was added to the cold solution and the mixture was allowed to warm to room temperature and left to stir for 12 hours. The mixture was transferred into a separatory funnel and the crude product was extracted into ethyl acetate. The organic phase was separated, dried ($MgSO_4$) and concentrated. The brominated product (BDP-3) was obtained by purifying the crude mixture via flash column chromatography (silica, 1:1 ethyl acetate:methanol) to yield

48 mg (0.091 mmol, 47.9% yield) of dark red crystalline powder. The final product was found to contain a persistent impurity (in $CDCl_3$: ^{1}HNMR δ=1.26 ppm; ^{13}CNMR δ=29.85 ppm) which arose due to the unconventionally high polarity of the eluent system used for purification. This was confirmed by running the clean eluent system through a column containing only silica and, after evaporating the collected fractions, the impurity was confirmed to originate from the silica column via ^{1}HNMR (Figure S5 inset). However, modification to the purification protocol for BDP-3 in order to avoid the impurity were unsuccessful. Importantly, the impurity had no apparent photochemistry associated with it, therefore was of no concern for this study.^{1}HNMR δ (400 MHz, $CDCl_3$): 1.26(impurity), 1.37(6H, s, CH_3), 2.63 (6H, s, CH_3), 7.45 (2H, d, J = 8Hz, phenyl), 8.29 (2H, d, J = 8Hz, benzene); figure S5. ^{13}C NMR δ (100 MHz, $CDCl_3$): 13.9, 14.0, 29.9 (impurity), 128.6, 130.0, 130.5, 131.3, 140.1, 140.5, 154.8, 169.4; figure S6. HRMS(ESI) *m/z*: calc. for $C_{20}H_{16}BF_2N_2O_2{}^{79}Br^{81}Br$ $[M-H]^+$: 524.9619, found: 524.9597.

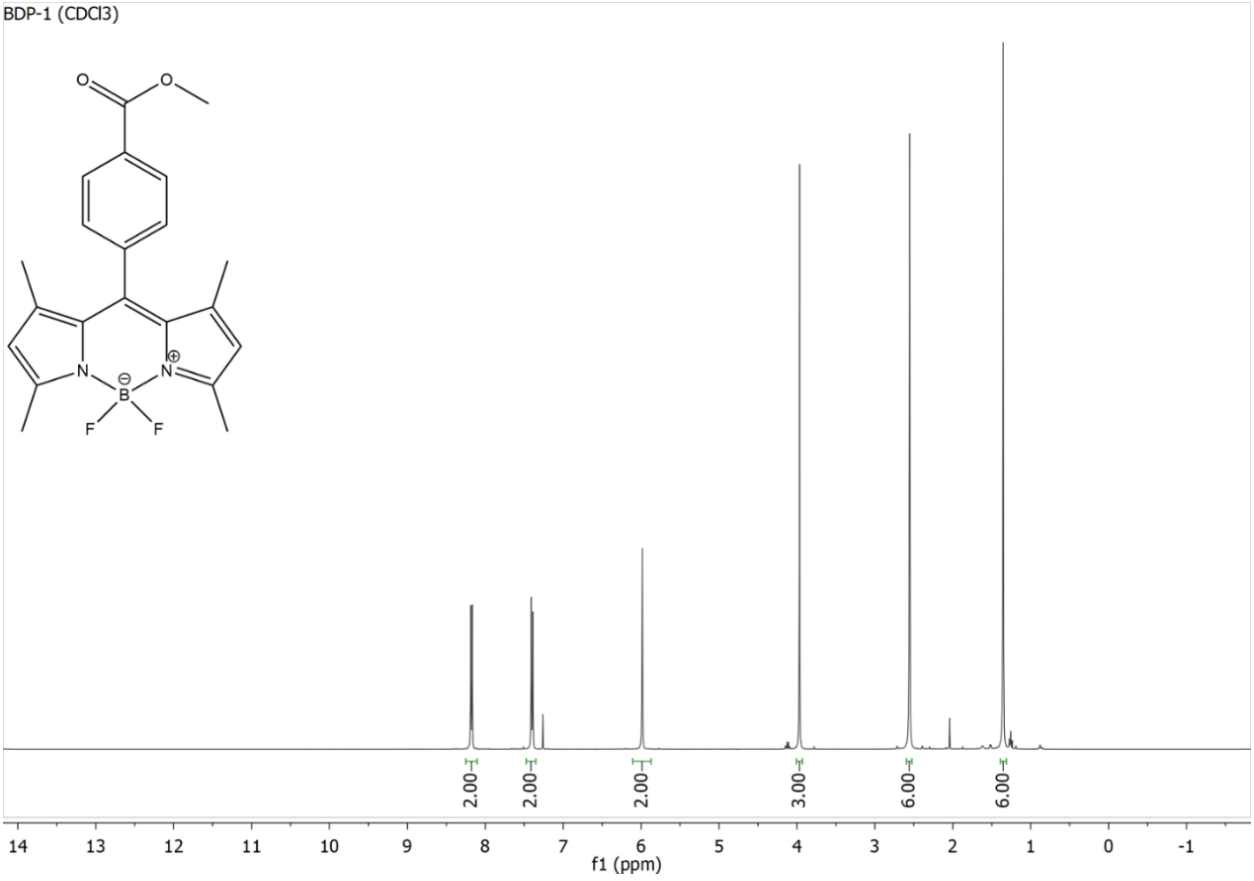

Figure S1: ^{1}HNMR of BDP-1 (400 MHz, $CDCl_3$)

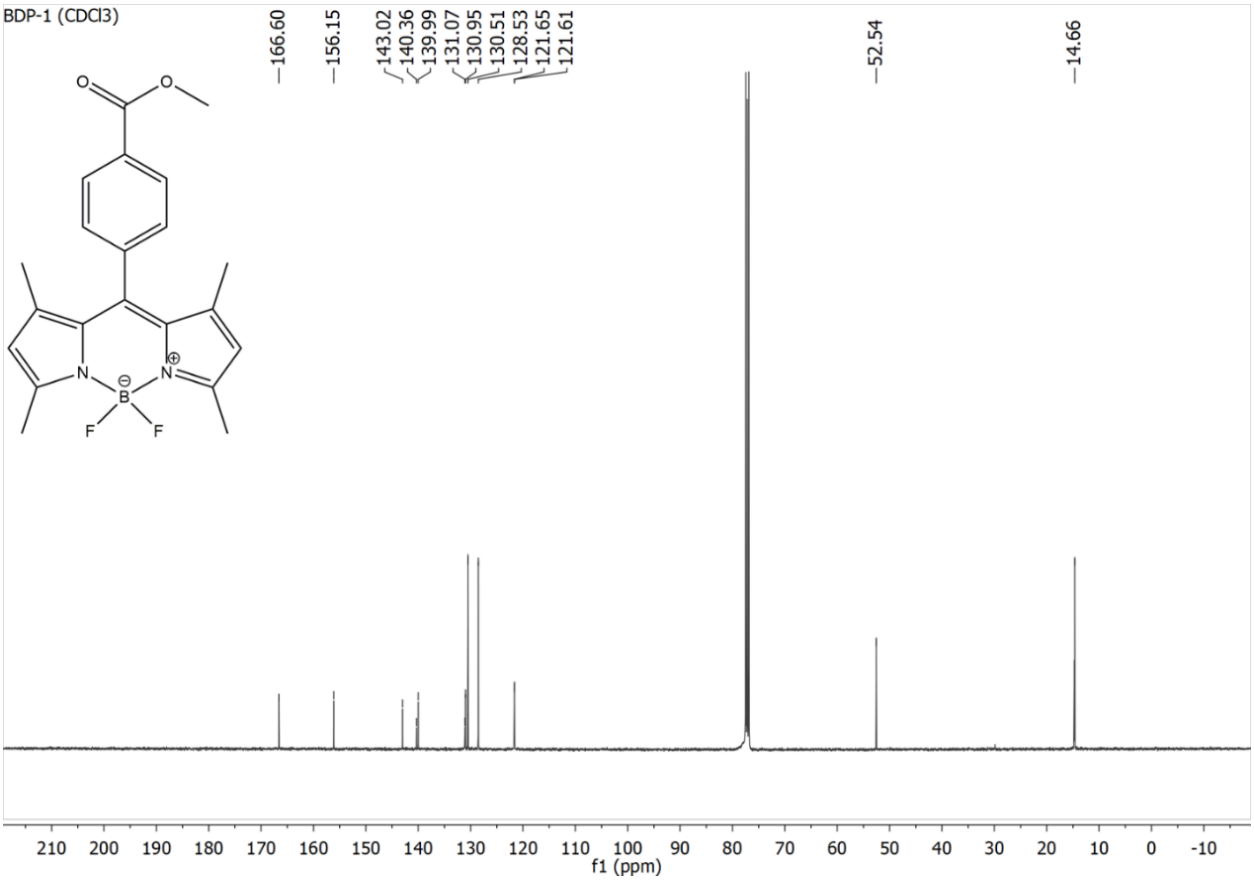

***Figure S2*:** ^{13}CNMR of BDP-1 (100 MHz, $CDCl_3$)

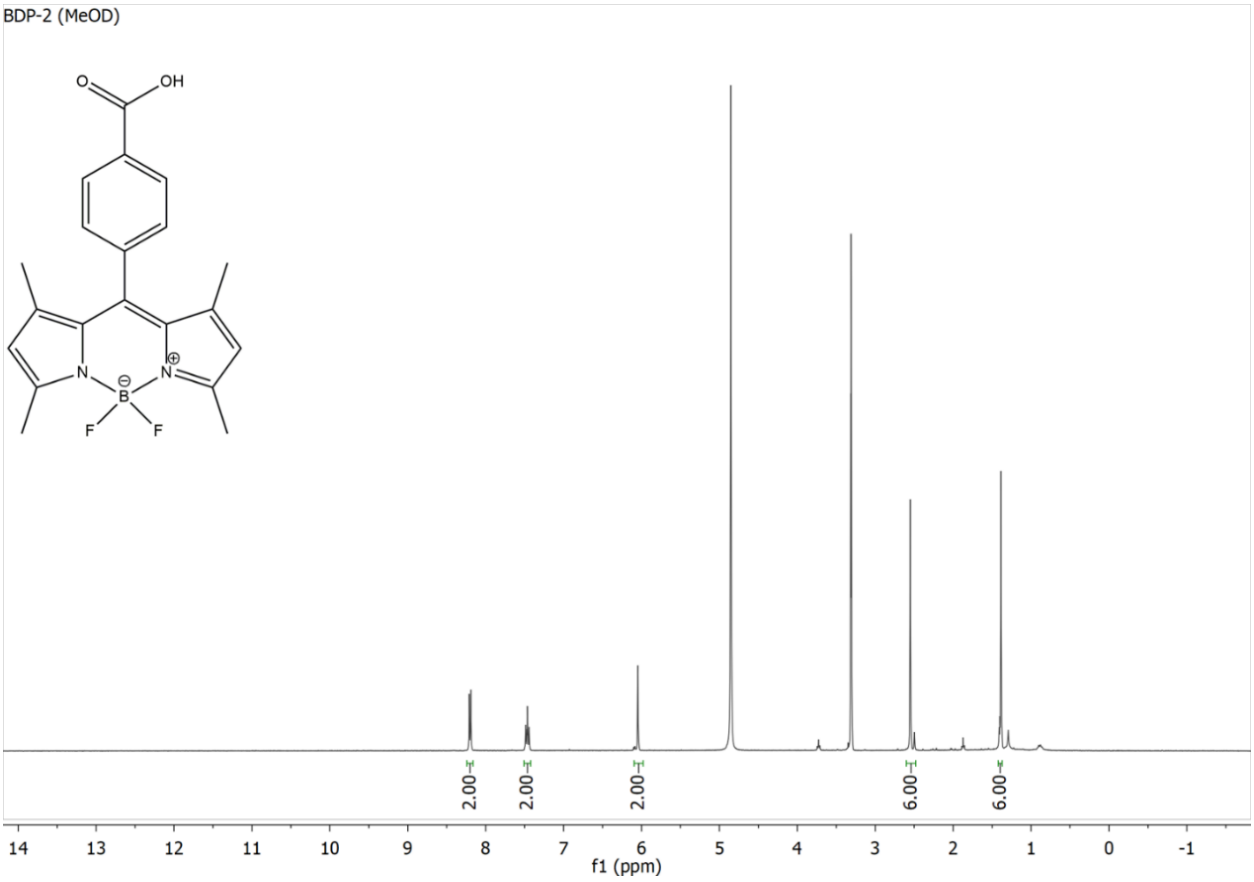

Figure S3: ^{1}HNMR of BDP-2 (400 MHz, MeOD)

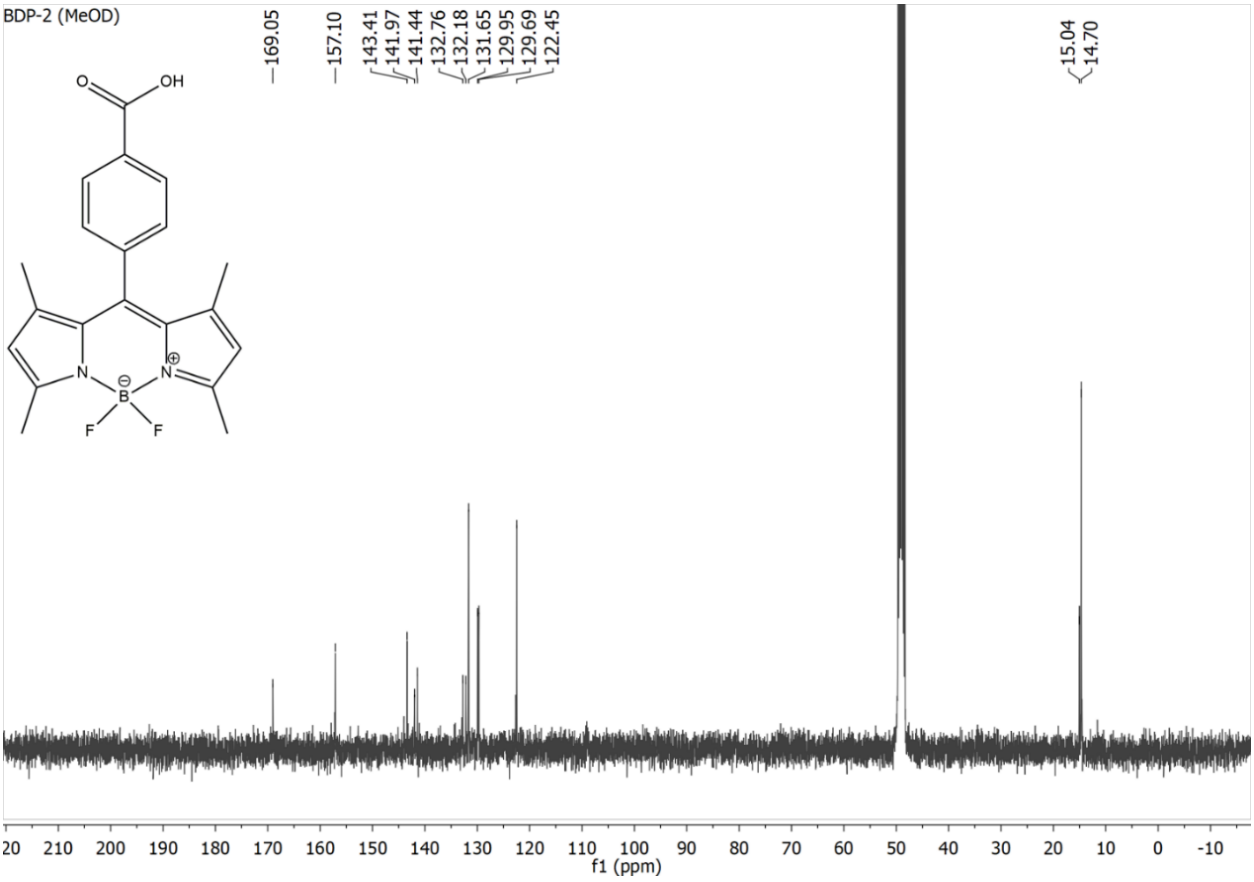

Figure S4: ^{13}CNMR of BDP-2 (100 MHz, MeOD)

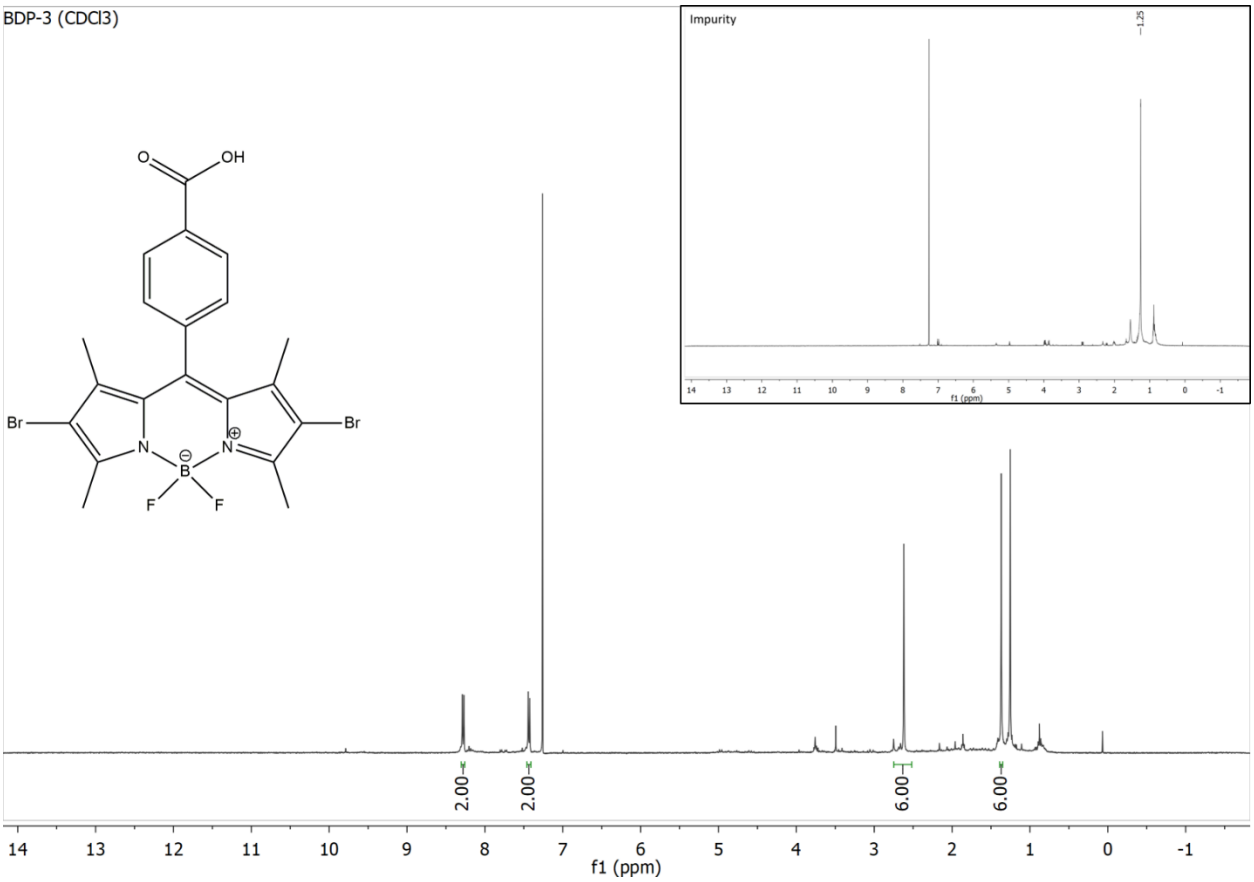

Figure S5: ^{1}HNMR of BDP-3 (400 MHz, $CDCl_3$). Inset: ^{1}HNMR of the impurity collected from silica column, present in BDP-3.

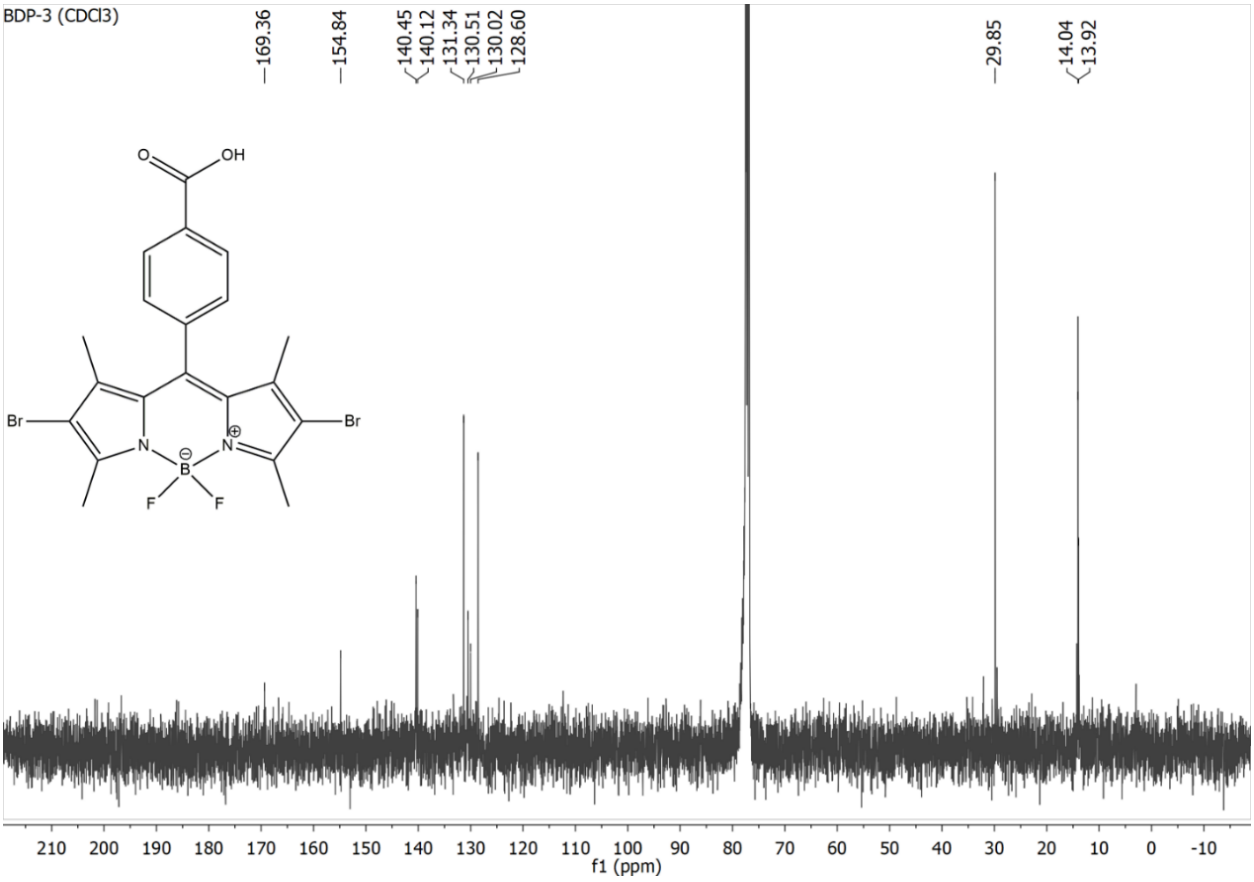

Figure S6: ^{13}CNMR of BDP-3 (100 MHz, $CDCl_3$)

1.2. Synthesis of PS-APTES.

All the photosensitizers were coupled to an alkoxysilane moiety (3-aminopropyl triethoxysilane – APTES) via an EDC (N-(3-dimethylaminopropyl)-N'-ethylcarbodiimide hydrochloride) promoted protocol.[5] In the case of Rose Bengal (RB) and erythrosine B (ERB) photosensitizers, the disodium salts of the dyes were first dissolved in water and acidified to pH of ~2 in order to obtain the protonated acid form of each dye.[6] Red precipitate formed in the acidic environment was collected via vacuum filtration and dried. 0.10 mmol of acidified RB or ERB, or BDP photosensitizer was dissolved in 6 mL of dry THF. To this solution 0.15 mmol of EDC in 4 mL of dry THF was added and the mixture was allowed to stir briefly under an atmosphere of argon. Then, 0.15 mmol of APTES was injected into the mixture and the coupling reaction was allowed to proceed at room temperature under argon atmosphere overnight. PS-APTES product formation in the reaction pot was confirmed via mass spectrometry. Due to severe moisture sensitivity of the aloxysilanes, the PS-APTES product was used for further nanoparticle formation directly from the reaction pot.

BDP-APTES: HRMS(ESI) *m/z*: calc. for $C_{29}H_{39}B^{81}Br\,^{79}BrF_2N_3O_4Si^+$ $[M+H]^+$: 731.1128, found: 731.1125.

ERB-APTES: HRMS(ESI) *m/z*: calc. for $C_{29}H_{28}I_4NO_7Si^-$ $[M-H]^-$: 1037.7819, found; 1037.7781.

RB-APTES: HRMS(ESI) *m/z*: calc. for $C_{27}H_{18}{}^{37}Cl^{35}Cl_3I_4NO_6Si^+$ $[M-CH_3CH_2OH]^{+\cdot}$: 1127.5837, found: 1127.6319.

1.3. Preparation of PS@SiO2 nanoparticles.

After stirring the PS-APTES reaction mixture overnight under inert atmosphere, a 0.10 mL aliquot of the solution containing the desired product was added to a mixture of 10 mL cyclohexane and 640 µl IGEPAL CO-520 surfactant, ensuring the concentration of the latter surfactant to be greater than its cmc value of 25 mM.[7, 8] The resulting cloudy and coloured mixture was thoroughly sonicated and while stirring, 164 µL of 28% aqueous ammonium hydroxide ($NH_4OH_{(aq)}$) and 110 µL of tetraethyl orthosilicate (TEOS) were added in sequence upon which the solution became clear. After stirring the mixture overnight, hybrid PS@SiO_2 nanoparticles were collected and purified via several centrifugation cycles (five 30 minute cycles at 10,000 rpm (~17,000 G) with supernatant removal and resuspension in fresh absolute ethanol after each cycle). The protocol yielded 20-25 mg of ~33 nm diameter PS@SiO_2 nanoparticles as characterized via transmission electron microscopy (TEM – see section 2.2 and figures S11, S12, S13). Surface charge of PS@SiO_2 nanoparticles was measured in ethanol using Zetasizer Nano (Malvern) instrument (λ_{ex} = 640 nm).

1.4. Preparation of pure SiO2 nanoparticles.

For consistency, pure silica nanoparticles were also prepared using the reverse microemulsion method. Briefly, 164 µL of a 28% aqueous ammonium hydroxide solution were added to a well-mixed solution of 10 mL cyclohexane and 640 µL IGEPAL CO-520. The mixture briefly turned cloudy, becoming clear upon sonication while also remaining colourless. Next, 110 µL of TEOS were added dropwise to the mixture

while stirring. The clear and colourless solution was left stirring, capped overnight. Pure SiO_2 nanoparticles were separated from the organic solvent and the surfactant by several rounds of centrifugation at 10, 000 rpm (~17, 000 G) for 30 minutes, where the supernatant was removed, and the nanoparticles were resuspended in fresh absolute ethanol with each successive cycle. The protocol yielded 20-25 mg of 35.8±2.4 nm diameter SiO_2 nanoparticles. Surface charge of unmodified SiO_2 nanoparticles was measured in ethanol using Zetasizer Nano (Malvern) instrument (λ_{ex} = 640 nm).

1.5. Control PS@SiO2 nanoparticles

Since PS-APTES conjugates are air and water sensitive, forming polymers upon prolonged air exposure, purification of these compounds was not possible and is not typically reported in the literature.[7] However, we have ensured PS-APTES synthesis reaction was successful by performing indirect control experiments. Two PS@SiO_2 nanoparticle synthesis solutions were set up in an identical fashion, but with one containing unmodified photosensitizer, while the second containing an equimolar amount of PS-APTES from the EDC coupling mixture. In both cases, coloured nanoparticles were initially obtained, however after several centrifugation cycles the nanoparticles synthesised with unmodified PS lost their colour by "leaking" the dye contents into the suspension solvent (ethanol). On the contrary, nanoparticles synthesised using PS-APTES conjugates retained their dye content after the first two centrifugation cycles and for the remainder of the purification protocol. Results of the PS@SiO_2 nanoparticles control synthesis experiments are shown in figures S7-S9.

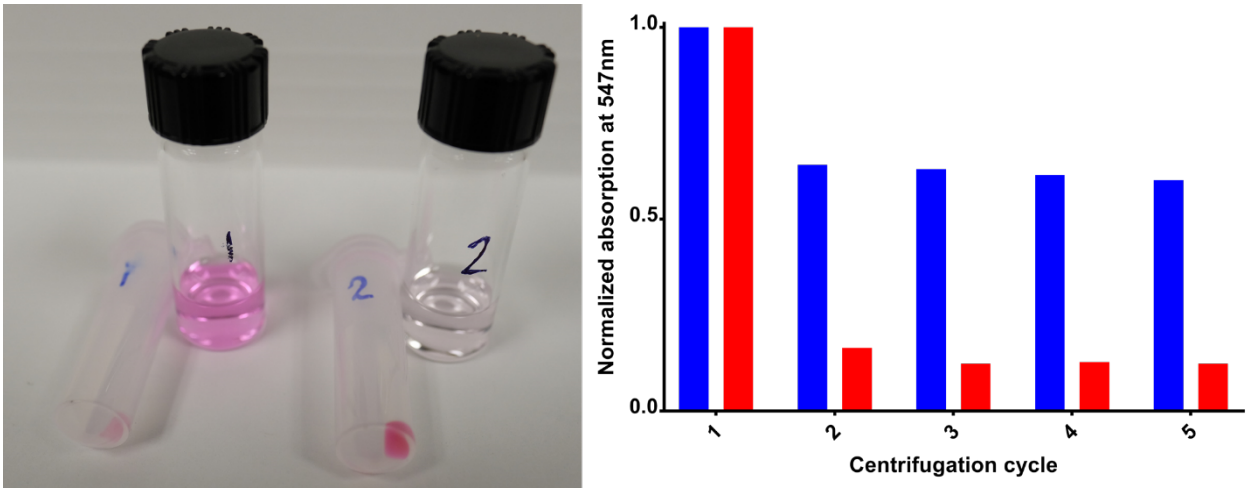

Figure S7: ERB@SiO_2 nanoparticle synthesis control. Photo: glass vials contain post-centrifugation supernatant extracted from plastic vials which contain the nanoparticle pellet. Photo taken after second centrifugation cycle. Label 1 represents the sample prepared using unmodified ERB, label 2 is for the sample made with ERB-APTES. The bar chart shows changes to the UV-Vis absorption of PS@SiO_2 nanoparticles prepared using ERB (red) or ERB-APTES (blue) upon multiple centrifugation/solvent replacement cycles; the data is normalized to the PS@SiO_2 absorbance after first centrifugation cycle.

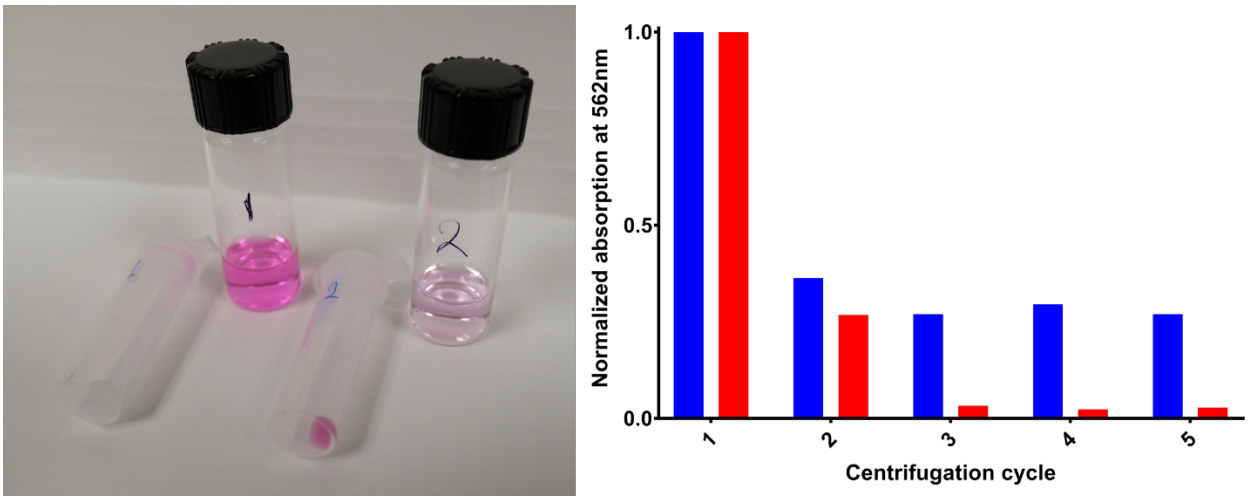

Figure S8: RB@SiO_2 nanoparticle synthesis control. Photo: glass vials contain post-centrifugation supernatant extracted from plastic vials which contain the nanoparticle pellet. Photo taken after third centrifugation cycle. Label 1 represents the sample prepared using unmodified RB, label 2 is for the sample made with RB-APTES. The bar chart shows changes to the UV-Vis absorption of PS@SiO_2 nanoparticles prepared using RB (red) or RB-APTES (blue) upon multiple centrifugation/solvent replacement cycles; the data is normalized to the PS@SiO_2 absorbance after first centrifugation cycle.

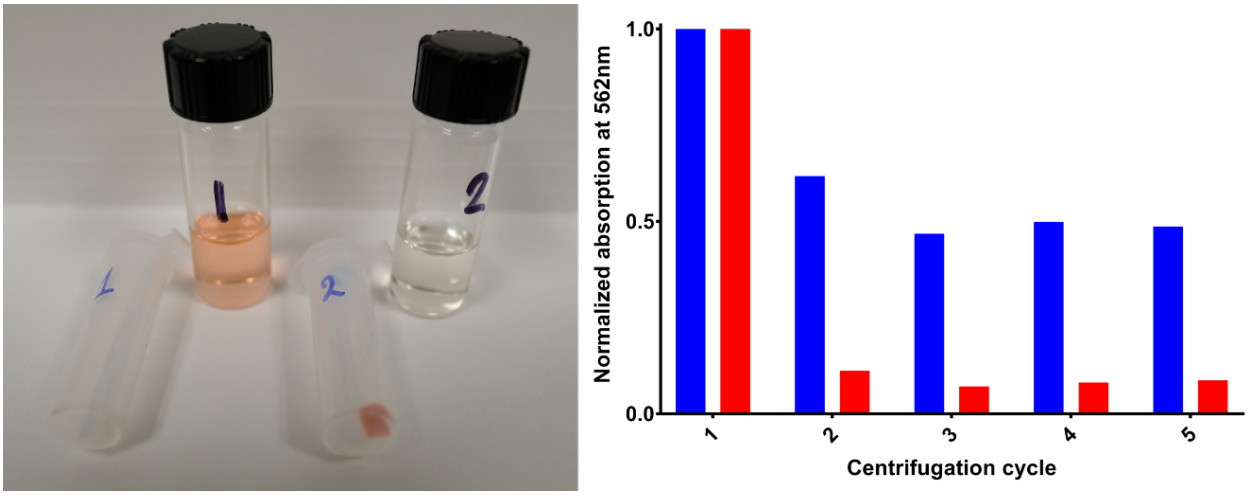

Figure S9: BDP@SiO_2 nanoparticle synthesis control. Photo: glass vials contain post-centrifugation supernatant extracted from plastic vials which contain the nanoparticle pellet. Photo taken after second centrifugation cycle. Label 1 represents the sample prepared using unmodified BDP, label 2 is for the sample made with BDP-APTES. The bar chart shows changes to the UV-Vis absorption of PS@SiO_2 nanoparticles prepared using BDP (red) or BDP-APTES (blue) upon multiple centrifugation/solvent replacement cycles; the data is normalized to the PS@SiO_2 absorbance after first centrifugation cycle.

2. General Procedures

2.1 Partition coefficients.

1-Octanol and phosphate buffered saline (PBS, pH=7.4) were mixed together in a separatory funnel at a 1:1 volume ratio in order to allow each solution to reach equilibrium with one another.[9] The solutions were mixed and allowed to separate overnight. The aqueous layer was removed for photosensitizer solution preparation, while the organic layer was used in subsequent steps. Each photosensitizer was dissolved/suspended in 2 mL of PBS. For RB, ERB and BDP photosensitizers, absorption was measured at 549 nm, 526 nm and 521 nm respectively. PBS solutions containing each dye were prepared to reach an optical density of ~0.7. This initial optical density was recorded and assigned a value of A_b. Then, 0.25 mL of PBS saturated 1-octanol was added to the photosensitizer solution and the suspension was agitated by shaking for 5 minutes. The resulting cloudy suspension was left in the dark overnight to settle. After separation, the UV-Vis absorption spectrum of the aqueous layer was taken and assigned a value of A_a. Using equation S1, values for partition coefficient (*log[P]*) were then calculated.[10]

$$\log[P] = \left(\frac{A_b}{A_a} - 1\right)\frac{V_{PBS}}{V_{oct}} \qquad \text{(S1)}$$

Where, V_{PBS} and V_{oct} are the volumes of PBS and 1-octanol used in partition experiment respectively. Figure S10 showcases the results of partition experiments.

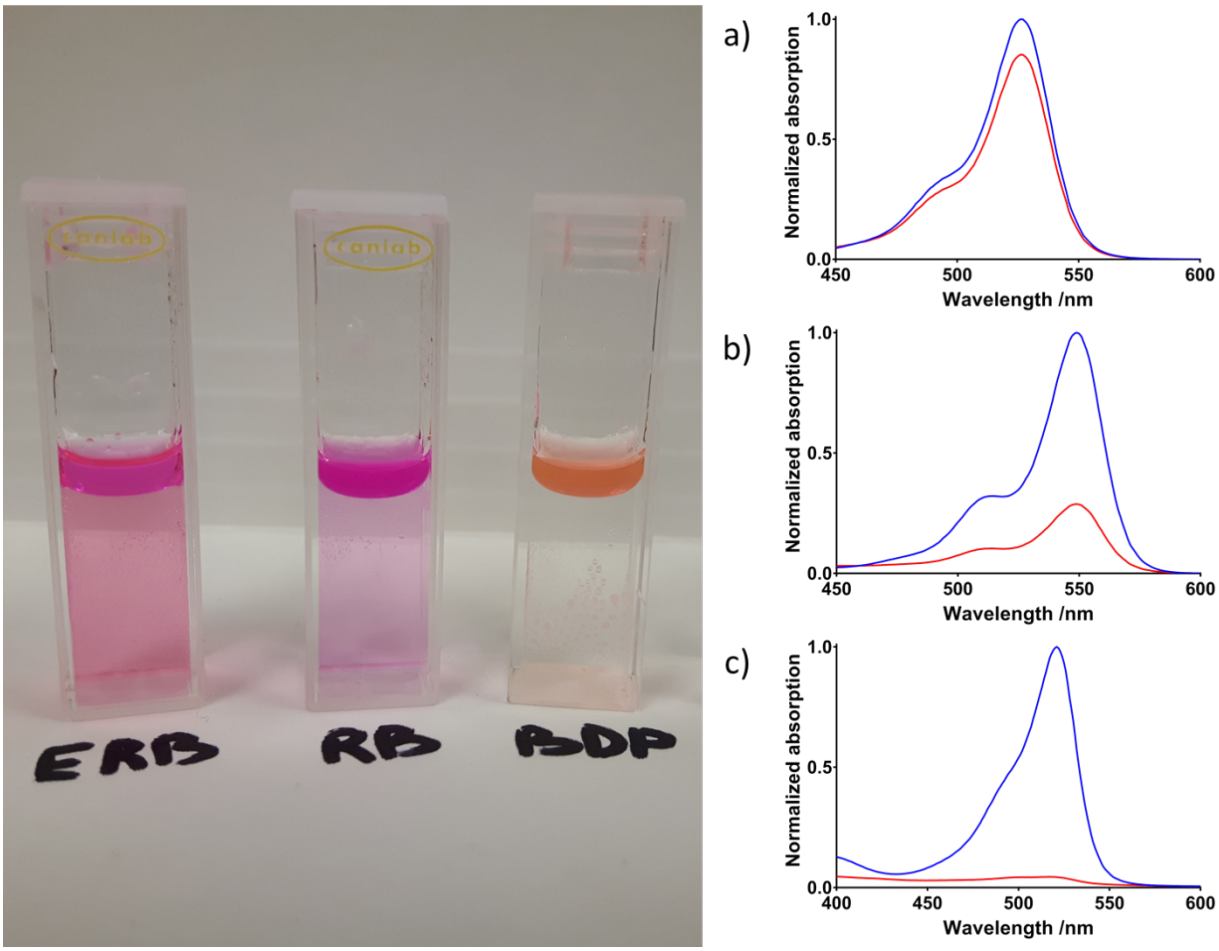

Figure S10: Photo – partition of the different photosensitizers between aqueous (bottom) and organic (top) phases. Inserts – UV-Vis absorption of aqueous phases for samples before (blue) and after (red) partition: ERB (a), RB (b) and BDP (c).

2.2. Nanoparticle characterization.

Nanoparticle sizes were characterized using transmission electron micrographs obtained on a TEM Hitachi H-7650 (Microscopy and Imaging Facility, University of Calgary). Samples were prepared on carbon-coated Cu TEM grids. Values for the diameter of the nanoparticles are based on at least 150 measurements. TEM images of the PS@SiO_2 nanoparticles and their size distribution histograms are shown in figures S11-S13.

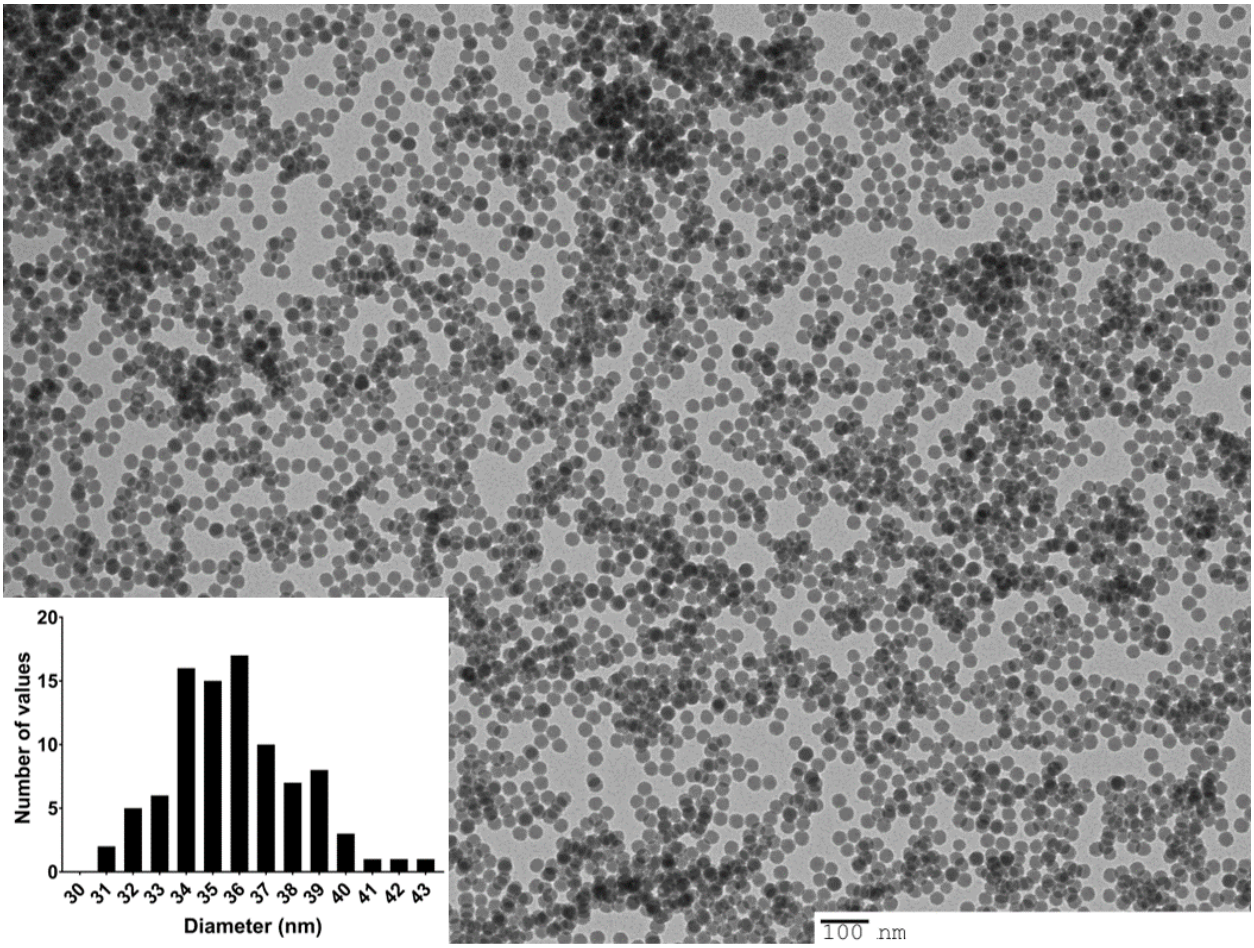

Figure S11: TEM image of ERB@SiO_2 nanoparticles, 35.8±2.4 nm diameter. Inset shows size distribution ERB@SiO_2 histogram.

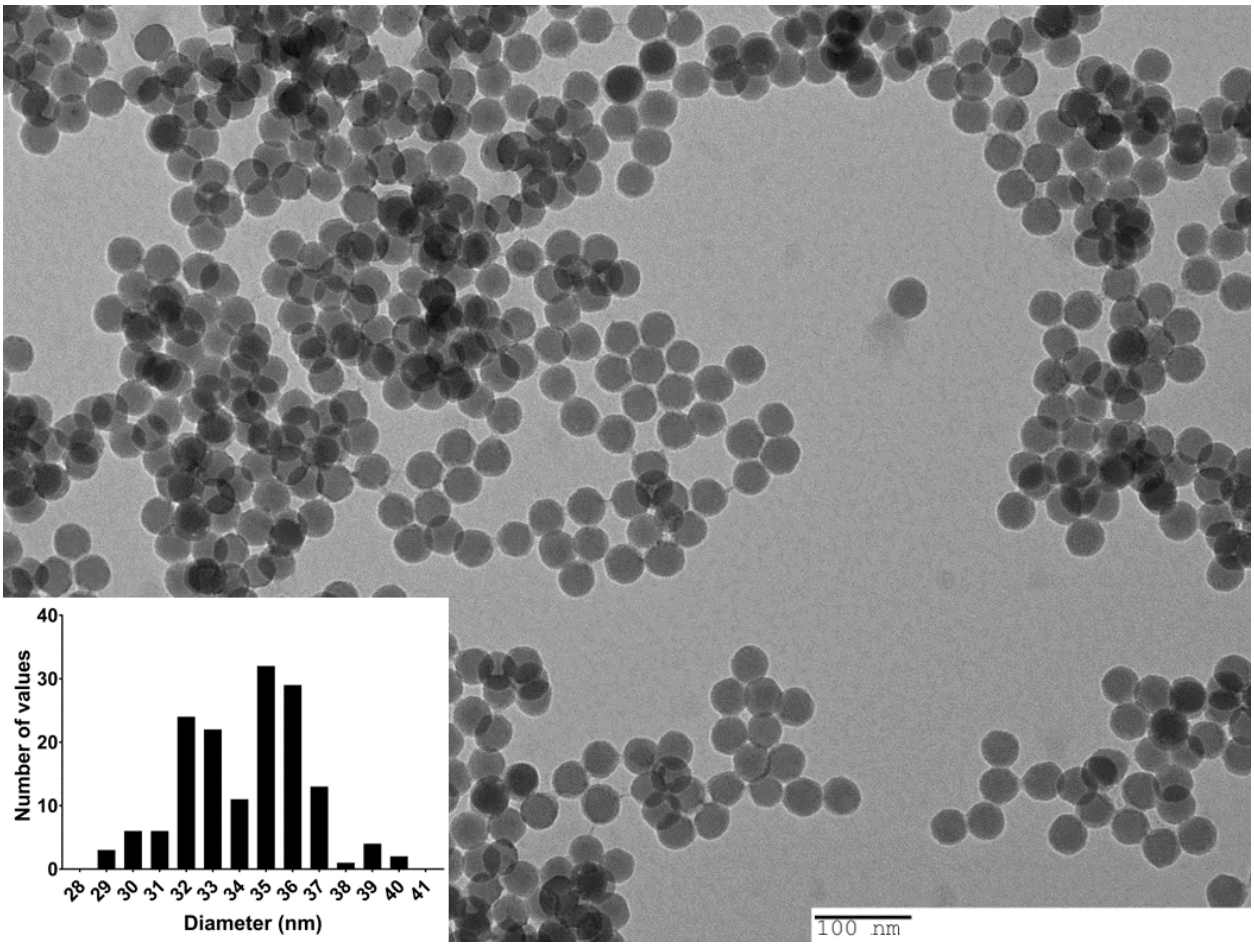

***Figure S12*:** TEM image of RB@SiO_2 nanoparticles, 34.2±2.3 nm diameter. Inset shows size distribution RB@SiO_2 histogram.

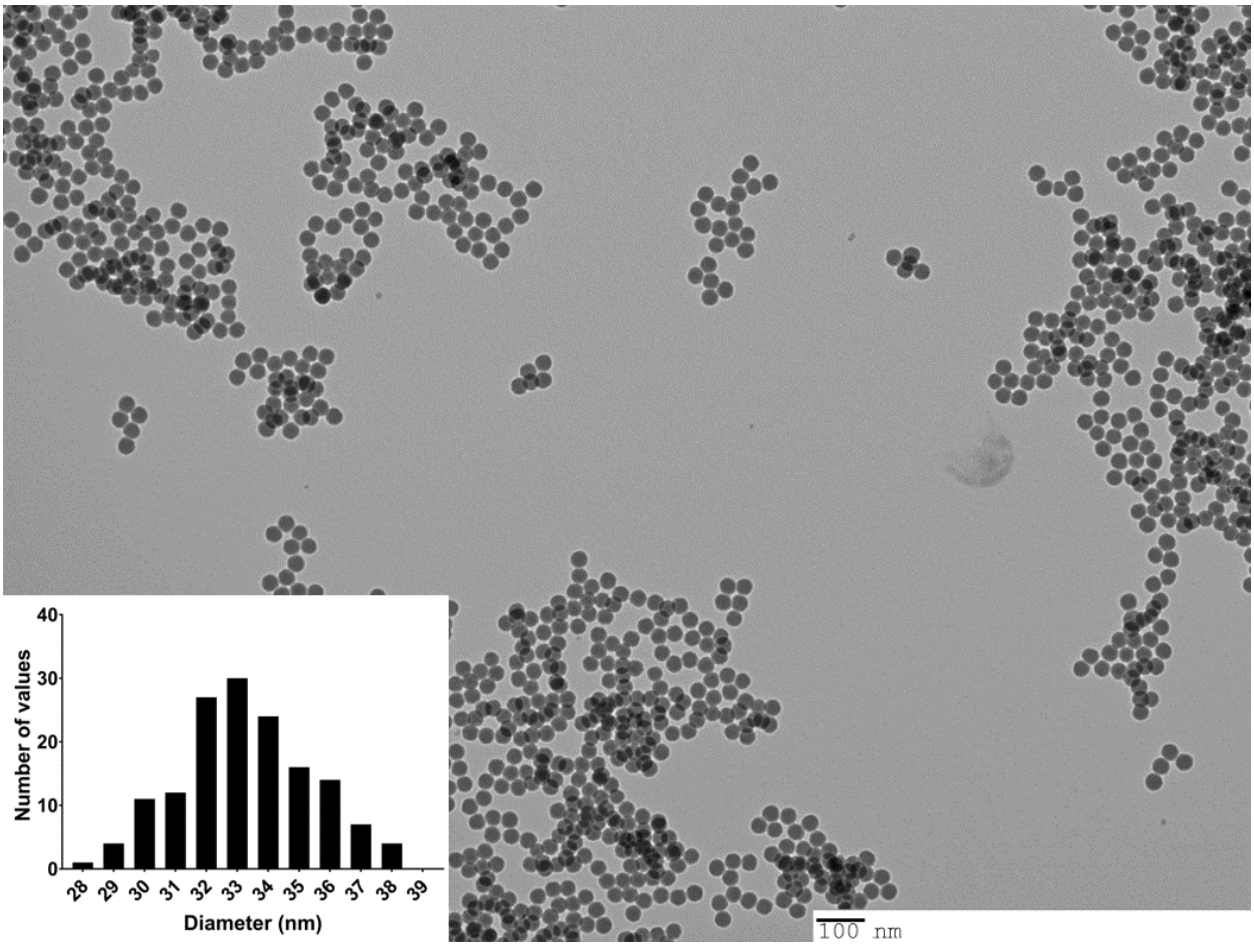

***Figure S13*:** TEM image of BDP@SiO_2 nanoparticles, 33.3±2.1 nm diameter. Inset shows size distribution BDP@SiO_2 histogram.

2.3. Dye loading in silica nanoparticles

In order to assess the dye loading of the various PS@SiO_2, the weight loss due to PS molecules was calculated from thermogravimetric analyses (TGA) for all the samples between 150°C after removal of physisorbed water and 900°C associated to the loss of PS (Figure S14a).[11] The data are summarized in the table below (Table S1). The difference in weight percent (Δwt%) for SiO_2 nanoparticles is only due to Si-OH condensation because no organic moieties are present in the sample. The difference weight percent due to PS is obtained by subtracting from the total Δwt% the value obtained for the Si-OH condenstation (10.79%). The TGA data for all PS@SiO_2 are presented in Figure S14b. The approximate number of dye per silica nanoparticles (dye loading) can be estimated from these TGA values by considering the mean nanoparticle volume derived from TEM images (Figures S11-13), and the density of amorphous silica (2.2g/cm^3) [12], as examplified below for ERB@SiO_2 with an average diameter of 35 nm.

$$NP_{volume} = \frac{4}{3}\,\pi\, r^3 = \frac{4}{3}\,\pi\,(17.5 \times 10^{-7}\ cm)^3 = 2.24\ \times\ 10^{-17}\ cm^3$$

$$NP_{weight} = \left(2.2\ \frac{g}{cm^3}\right) \times\ (2.24\ \times\ 10^{-17}\ cm^3) = 4.94\ \times\ 10^{-17}\ g$$

$$ERB_{weight\ per\ NP} = (\Delta wt\%\ from\ TGA)\ \times\ (weight\ of\ 1\ NP) =\ 0.0498\ \times\ (4.94\ \times\ 10^{-17}\ g)$$
$$= 2.46\ \times\ 10^{-18}\ g$$

If one consider the molecular weight of ERB to be 837.91 g/mol and N_A represents the Avogadro's number, then the average number of molecule is given by

$$Average\ number\ ERB = \frac{2.46 \times 10^{-18}\ g}{337.91\ g/mol} \times\ N_A = 1770\ \cong\ 1800$$

Table S1: Weight loss due to organic contain calculated from TGA

	wt% at 150 ℃	*wt% at 900 ℃*	*Δwt%*	*Δwt% due to PS*	*Average number of PS per NP*
SiO_2	94.65	83.86	10.79	-	-
ERB@SiO_2	96.79	81.02	15.77	4.98	~1800
RB@SiO_2	94.59	80.98	13.61	2.82	~800
BDP@SiO_2	96.03	81.61	14.42	3.63	~1900

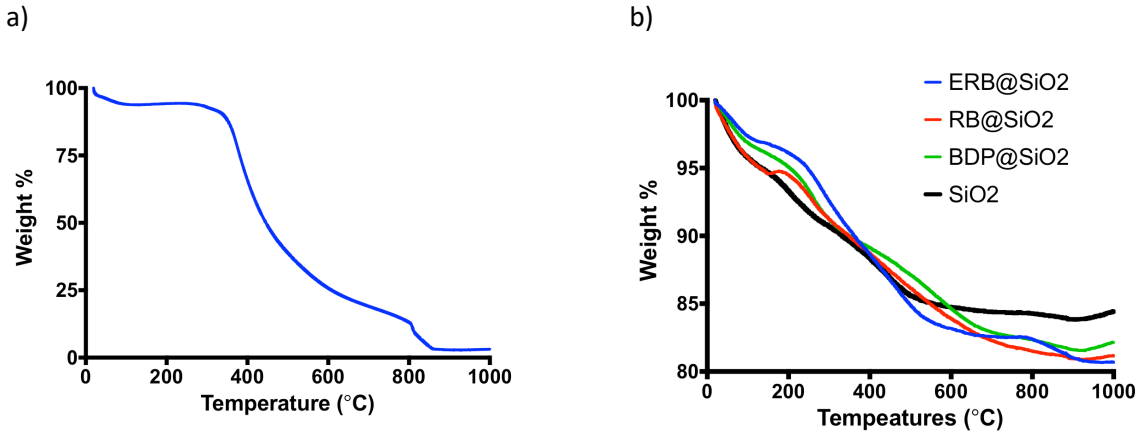

Figure S14: TGA curves of calcinated a) free RB, as dye representative; b) PS@SiO_2 nanoparticles. TGA measurements were performed under N_2 atmosphere with a heating rate of 2°C/min.

2.4. Photophysical characterization of PS and PS@SiO2.

UV-Vis absorption spectra were collected using Varian Cary 50 spectrophotometer. UV-Vis spectra, deconvoluted from the SiO_2 scattering profiles, are shown in figures S15-S17. Steady state fluorescence emission spectra were collected using PTI QuantaMaster 8000 fluorimeter. For ERB and ERB@SiO_2 samples the excitation was set at 488 nm; for RB and RB@SiO_2 at 530 nm; for BDP and for BDP@SiO_2 at 490 nm. Fluorescence emission spectra deconvoluted from the SiO_2 scattering profiles are shown in figures S15-S17. Fluorescence lifetimes for PS@SiO_2 samples were collected using Edinburgh FLS900 fluorescence spectrometer with an excitation wavelength set at 530 nm and 545 nm for ERB and ERB@SiO_2 samples respectively; 550 nm and 560nm for RB and RB@SiO_2 samples respectively; and 540 nm and 525 nm for BDP and BDP@SiO_2 samples respectively. The instrument-response function (IRF) was recorded at the appropriate excitation wavelengths by using a dilute solution of Ludox. The fluorescence decays were analyzed by using the software package provided by Edinburgh Instruments. Re-convolution of the IRF to the calculated decay was necessary to take into account the width of the excitation pulse. The decay data for the free dyes were all found to be mono-exponential and were fitted with a single exponential function. On the other hand, the emission decays for all PS@SiO_2 were fitted with a sum of two exponentials (Equation S2), where A_i corresponds to the pre-exponential factor of species "*i*" and k_i corresponds to the decay rate constant of the excited state of "*i*", which is equal to the inverse of its lifetime. The sum of all pre-exponential factors (A_i) was normalized to unity, and the magnitude of each pre-exponential factor is related to the abundance of that species.

$$I(t) = I_0 \sum_{i=1}^{2} A_i \, e^{-k_i t} \quad \text{(S2)}$$

The goodness of the fit was judged by the χ^2 values recovered for the fit of the experimental data to equation S2. Fits were considered adequate for χ^2 values between 0.9 and 1.2. Fluorescence lifetime decays for samples in water are shown in figure S18-S20, with analysis details given in table S2.

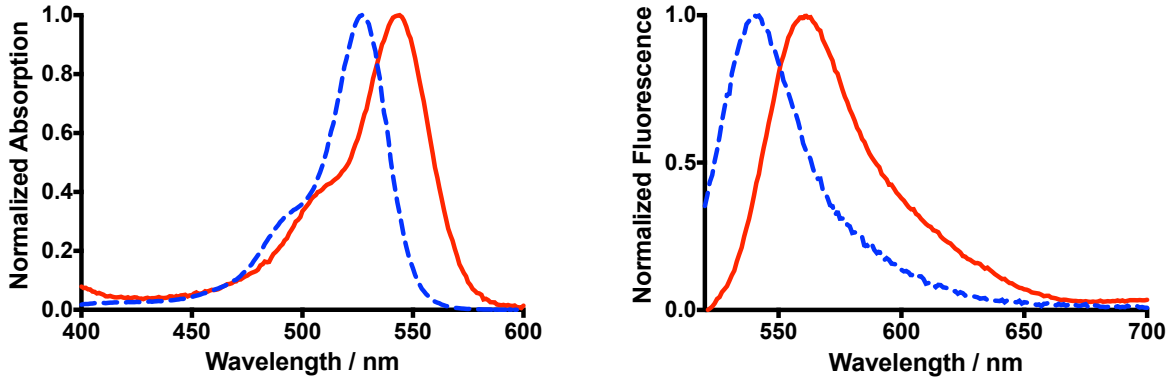

Figure S15: Normalized UV-Vis absorption spectra (left) and fluorescence emission spectra (right) for samples of erythrosine B (dashed blue) and ERB@SiO_2 (red) in water.

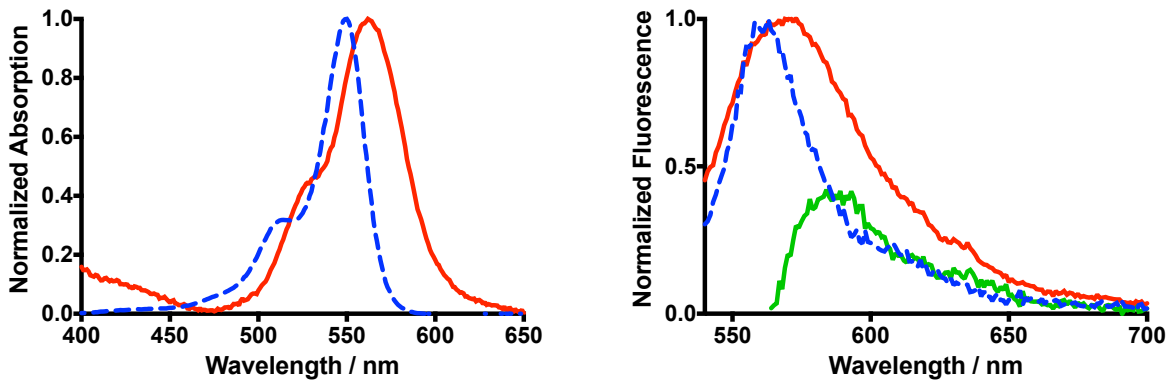

Figure S16: Normalized UV-Vis absorption spectra (left) and fluorescence emission spectra (right) for samples of Rose Bengal (dashed blue) and RB@SiO_2 (red) in water. The green spectrum on the right panel corresponds to the spectral difference between RB@SiO_2 and RB free in solution.

ERB exhibited a red-shift of about 16 nm in both its absorption and fluorescence emission spectra upon encapsulation within the silica matrix (see Figures S15). According to the literature, this bathochromic shift originated from a confinement effect, where strong interaction with the silica matrix distorted the dye's conformational geometry.[13] RB presented a similar bathochromic shift of about 13 nm in its absorption spectrum, which was accompanied by an overall broadening of spectral envelop and an increase of the relative intensity of the shoulder to the main peak (Figure S16). This result was indicative of some sort of dye aggregation within the silica matrix.[14] On the other hand, the emission signature of RB@SiO_2 remained similar to free RB in water, albeit for a broadening of the emission envelope, corresponding to an increase of about 10 nm of the full width at half maximum (Figure S16). By subtracting the emission signal recorded for the free dye in water from the one obtained for RB@SiO_2, a novel fluorescence spectrum is obtained with a maximum emission located at around 583 nm (Figure S16). This difference spectrum was similar to the one reported in the literature for RB incorporated in mesostructured silica.[13]

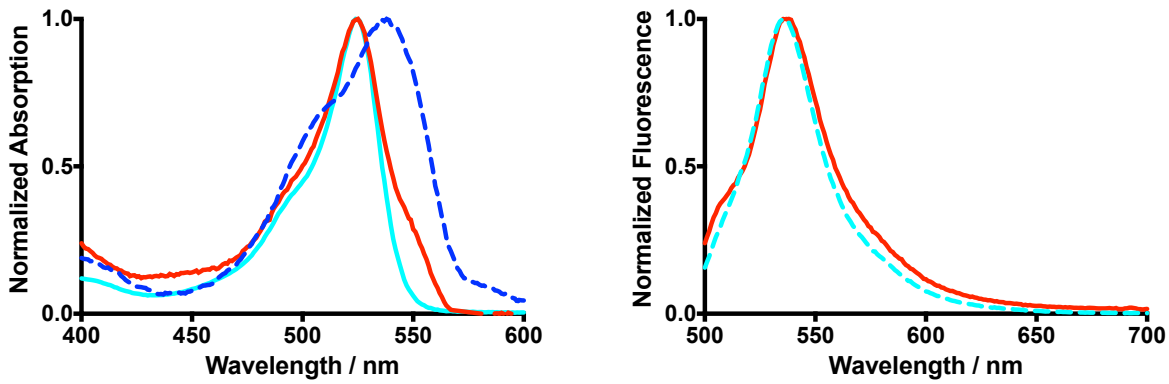

***Figure S17*:** Normalized UV-Vis absorption spectra (left) and fluorescence emission spectra (right) for samples of the free BDP dye (BDP-3 in synthetic procedure) (dashed blue) in H_2O; BDP@SiO_2 (red) in H_2O; and BDP-3 in EtOH.

Free BDP in water was found to have a broad UV-Vis absorption signature characteristic of an aggregated dye in aqueous solution (Figure S17). On the other hand, the absorption spectrum of BDP@SiO_2 was significantly blue shifted compared to the one found in aqueous solution. In fact, it matched very well the spectrum of the free dye in ethanol, where it is present as a monomeric species (Figure S17).

Table S2: Fluorescence lifetime analysis for PS@SiO_2 nanoparticle systems.[†]

	τ_1/ns	τ_2/ns	A_1/%	A_2/%	χ^2
ERB [(a)]	0.091±0.009	-	100	-	1.040
ERB@SiO₂ [(a)]	0.087±0.001	0.322±0.007	88.5±0.6	11.5±0.3	0.989
RB [(a)]	0.080±0.0001	-	100	-	1.001
RB@SiO₂ [(a)]	0.111±0.001	0.606±0.001	96.3±0.2	3.7±0.3	0.983
BDP (BDP-3) [(b)]	0.822±0.004	-	100	-	0.990
BDP@SiO₂ [(a)]	0.895±0.005	1.97±0.06	94±1	6.3±0.6	0.918

[†] All values reported are based on triplicate measurements with standard deviation given by ± value. [(a)] Measurements performed in water. [(b)] Measurements performed in ethanol.

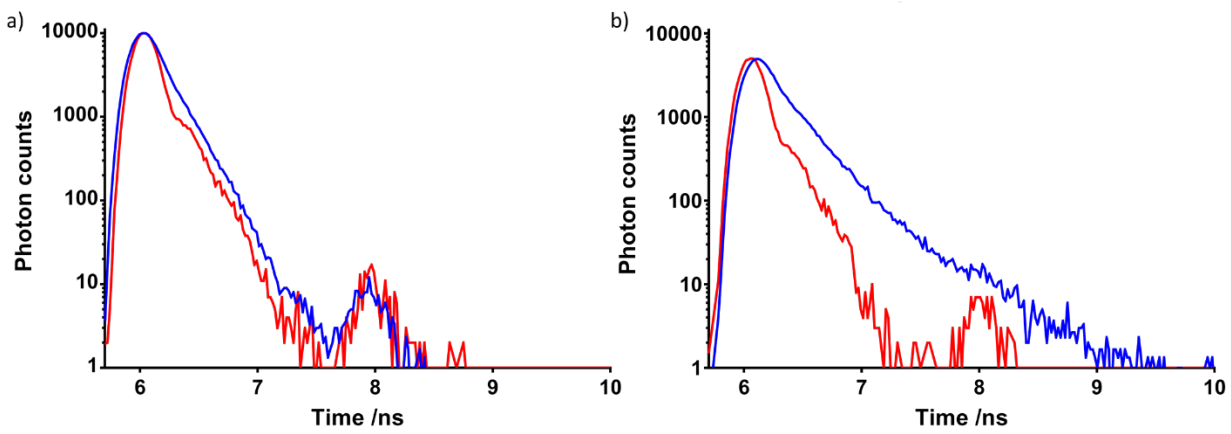

Figure S18: Fluorescence lifetime decays for samples of ERB (a) and ERB@SiO_2 (b) in water. Blue curve is for the sample measurement, red curve is the IRF.

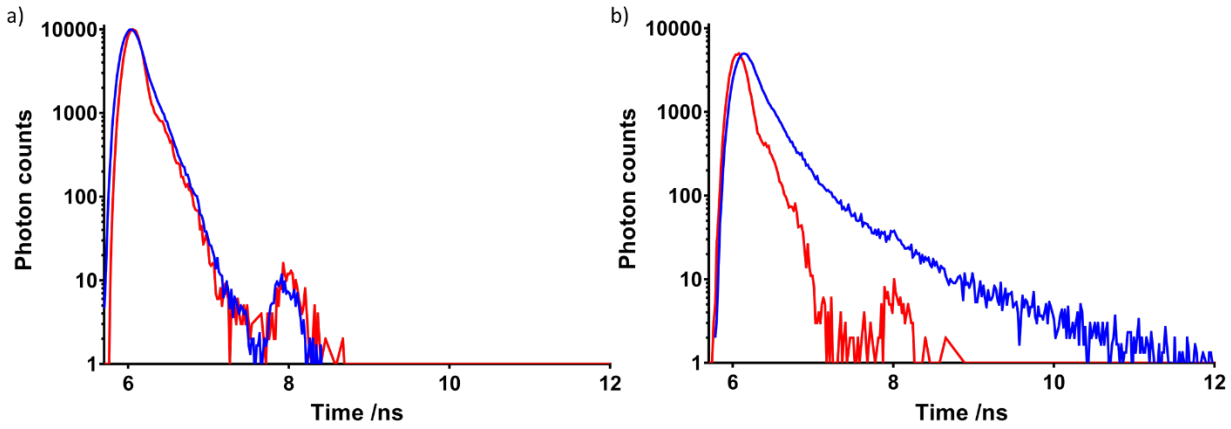

Figure S19: Fluorescence lifetime decays for samples of RB (a) and RB@SiO_2 (b) in water. Blue curve is for the sample measurement, red curve is the IRF.

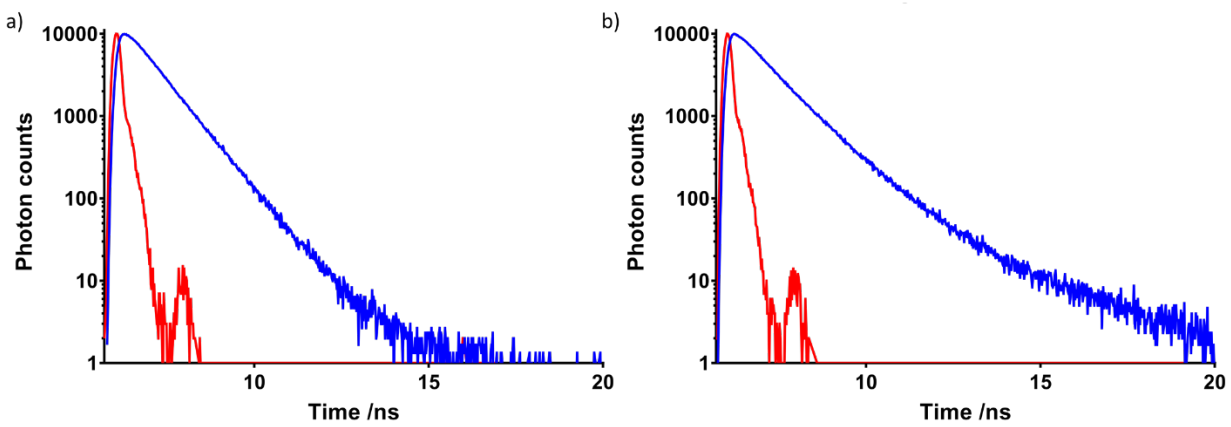

Figure S20: Fluorescence lifetime decays for samples of BDP-3 (a) in ethanol and BDP@SiO_2 (b) in water. Blue curve is for the sample measurement, red curve is the IRF.

2.5. Fluorescence quenching experiments.

The steady-state fluorescence emission spectra of PS and PS@SiO2 were collected in the absence and in the presence of various concentration of the fluorescent quencher NH_4I using a PTI QuantaMaster 8000 fluorimeter. For all samples, excitation was set at 510 nm. Fluorescence emission spectra of PS@SiO_2 were deconvoluted from the SiO_2 scattering profiles. Ammonium iodide (NH_4I) was used as a quencher instead of the more conventional potassium iodide (KI), as potassium appeared to favor the aggregation and precipitation of the nanoparticles, which could readily be observed by an increase in the turbidity of the sample. The Stern-Volmer and modified Stern-Volmer plots for two populations of fluorophores are presented in figures S21-S23.[15]

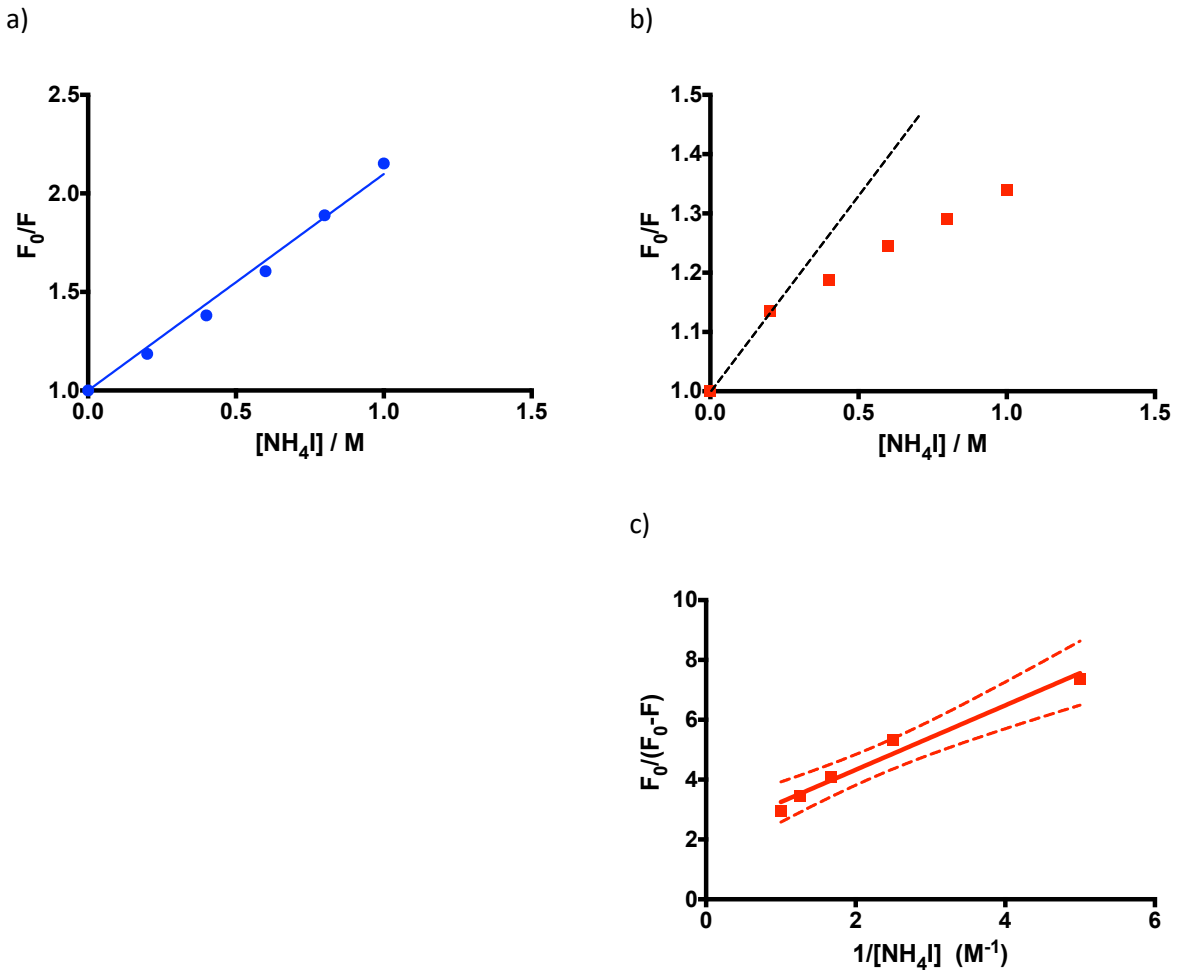

Figure S21: Stern-Volmer plot for the quenching of: a) ERB in H_2O (blue circles, K_D = 1.1 M^{-1}); and b) ERB@SiO_2 in H_2O (red squares). A dashed line has been added to guide the eye and highlight the downward curving of the plot. c) Modified Stern-Volmer plot for two populations of ERB@SiO_2 fluorophores, and accessible fraction with K_a = 2 M^{-1} and f_a = 0.45, and an inaccessible fraction with K_b = 0 M^{-1}. The dashed curve lines represent the 95% confidence bands of the best-fit line.

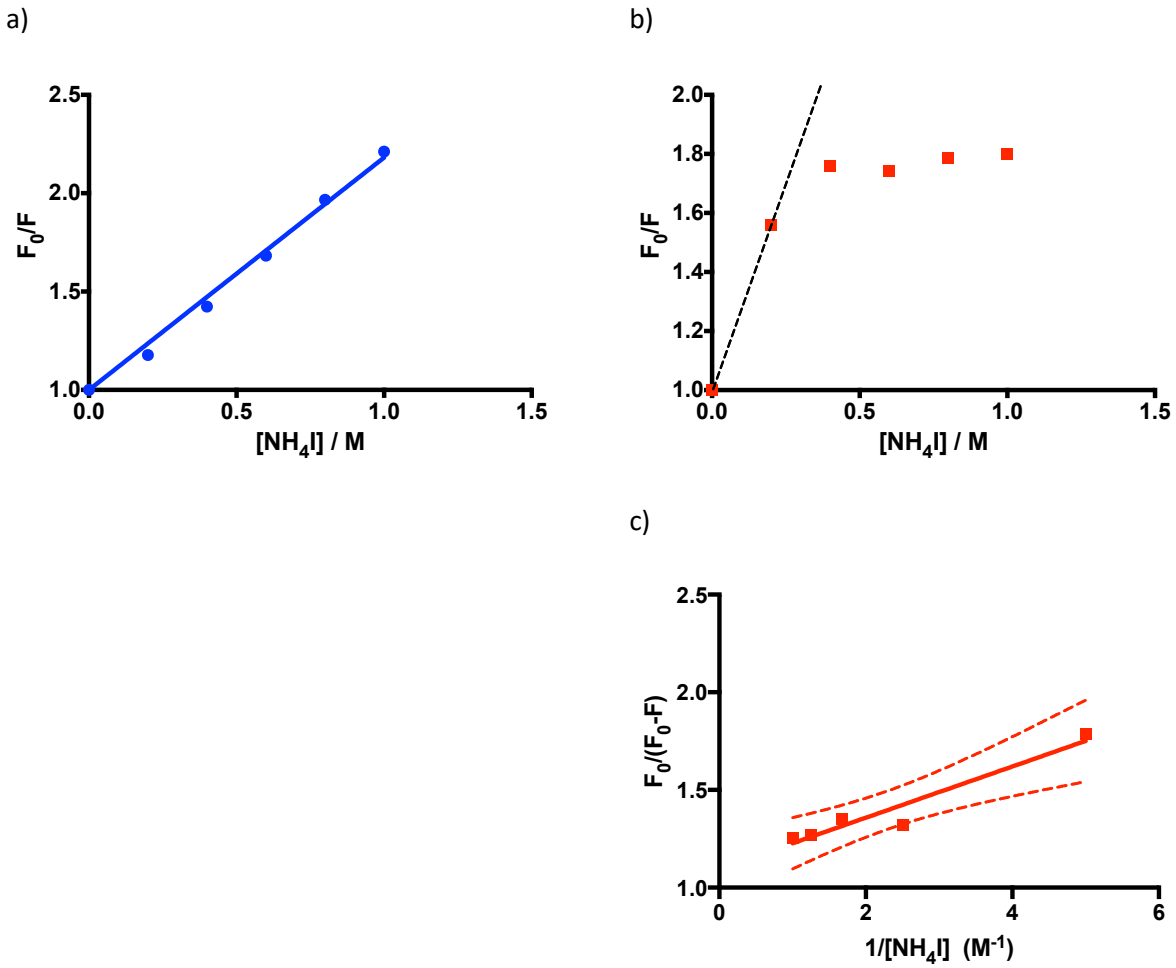

Figure S22: Stern-Volmer plot for the quenching of: a) RB in H_2O (blue circles, K_D = 1.2 M^{-1}); and b) RB@SiO_2 in H_2O (red squares). A dashed line has been added to guide the eye and highlight the downward curving of the plot. c) Modified Stern-Volmer plot for two populations of RB@SiO_2 fluorophores, and accessible fraction with K_a = 8 M^{-1} and f_a = 0.91, and an inaccessible fraction with K_b = 0 M^{-1}. The dashed curve lines represent the 95% confidence bands of the best-fit line.

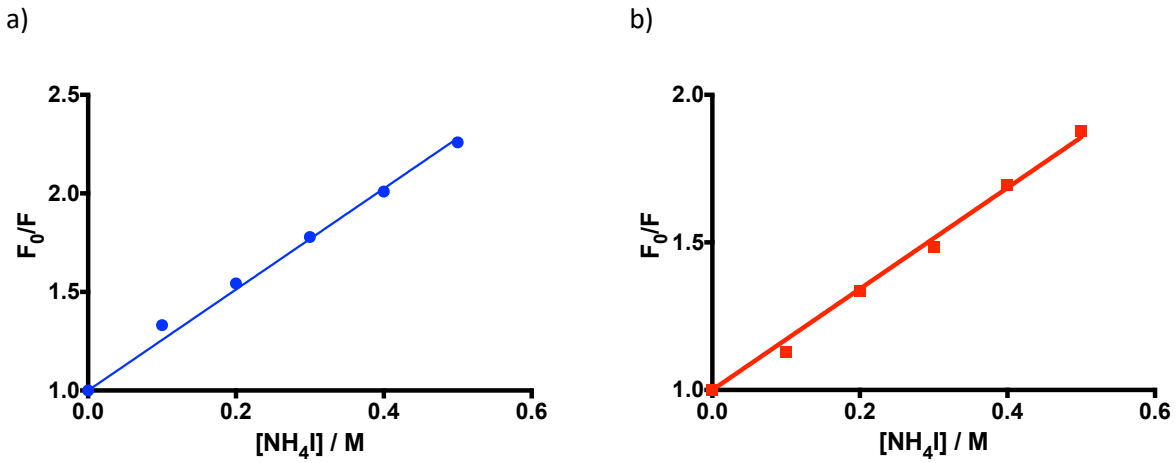

Figure S23: Stern-Volmer plot for the quenching of: a) BDP-3 in EtOH (blue circles, K_D = 2.6 M^{-1}); and b) DPB@SiO_2 in H_2O (red squares, K_D = 1.7 M^{-1}).

2.6. Nitrogen adsorption analysis.

The adsorption isotherms and pore size distributions for N_2 (99.999%) were conducted using an Accelerated Surface Area & Porosimetry System (ASAP) 2020 supplied by Micromeritics Instruments Inc. The sample (~200 mg of PS@SiO_2) suspended in methanol was loaded into the glass analysis tube and the sample was heated until dry while open to air. The tube was then heated under vacuum on a Schlenk line (~10^{-2} mbar) at 100 °C for 16 hours before being transferred to the ASAP 2020. The sample was heated under vacuum (~10^{-6} mbar) in two stages, initially to 60 °C at 1 °C min^{-1} for 2 hours then to 100 °C at 1 °C min^{-1} for 16 hours. After this the outgas rate was less than 1 µbar hr^{-1}. The sample was then backfilled with N_2 before being transferred to the analysis port where it was evacuated for at least a further 120 minutes before the analysis was started. The average pore volumes were obtained from the adsorption branch by using the Barret, Joyner and Halenda (BJH) formula with a Kruk-Jaroniec-Sayari (KJS) correction using isotherm adsorption data at relative pressure (P/P_0) from 0.000002198 to 0.413206297 (Figure S24).[16, 17] Surface areas of PS@SiO_2 and pure SiO_2 nanoparticles were obtained using Brunauer–Emmett–Teller (BET) theory[18] to be 108.7 m^2 g^{-1} (ERB@SiO_2), 135.7 m^2 g^{-1} (RB@SiO_2), 120.9 m^2 g^{-1} (BDP@SiO_2), and 123.0 m^2 g^{-1} (pure SiO_2).

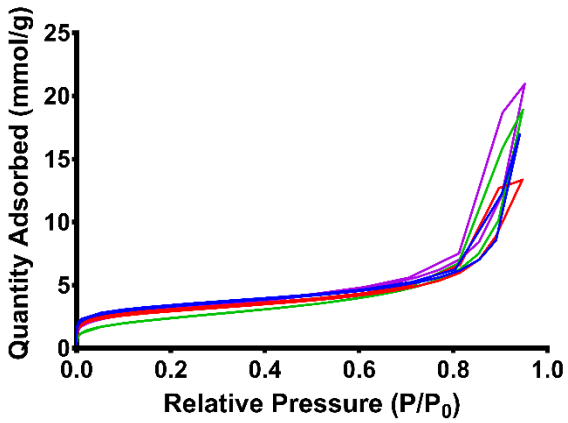

Figure S24: N_2 adsorption/desorption isotherms obtained from RB@SiO_2 (purple), ERB@SiO_2 (red), BDP@SiO_2 (green) and pure SiO_2 (blue) nanoparticles.

2.7. Direct detection of singlet oxygen luminescence.

The specific near-infrared phosphorescence kinetics of $^1O_2$ was detected by means of a customized system. A diode-pumped pulsed Nd:YAG laser (FTSS355-Q, Crystal Laser, Berlin, Germany) working at 1 kHz repetition rate at 532 nm (12 mW, 1.2 µJ per pulse) was used for excitation. A 1064 nm rugate notch filter (Edmund Optics, York, U.K.) was placed at the exit port of the laser to remove any residual component of its fundamental emission in the near-infrared (NIR) region. The $^1O_2$ luminescence exiting from the sample was detected at 90° angle via an Hamamatsu NIR detector (peltier cooled at -62.8°C operating at 800 V) coupled to a grating monochromator (Spectral Products, CM110). Photon counting was achieved with a multichannel scaler (NanoHarp 250, PicoQuant Gmbh, Germany).

The production of $^1O_2$ via photosensitization is essentially a two-step process in which light energy is first absorbed by a photosensitizer (PS) and then transferred to molecular oxygen to produce $^1O_2$. This process can be adequately modelled by Scheme S2 presented below. Absorption of light by PS promotes it to its excited singlet state ^{1}PS, which evolves over time (k_{ISC}) to the lower-lying triplet excited state, ^{3}PS, in competition with radiative (fluorescence, k_F) and non-radiative (internal conversion, k_{IC}) decay back to the ground state. ^{3}PS may then transfer its energy to molecular oxygen to produce $^1O_2$ or decay back to the ground state (k_T). Therefore, the rate of $^1O_2$ production is equal to the rate of ^{3}PS decay, and the time constant of the process is therefore the triplet lifetime τ_T *(= 1/k_T)*. Once produced, $^1O_2$ will disappear with a lifetime, τ_Δ, mostly through non-radiative processes, but a minor fraction of $^1O_2$ molecules will emit a photon in the near-IR.

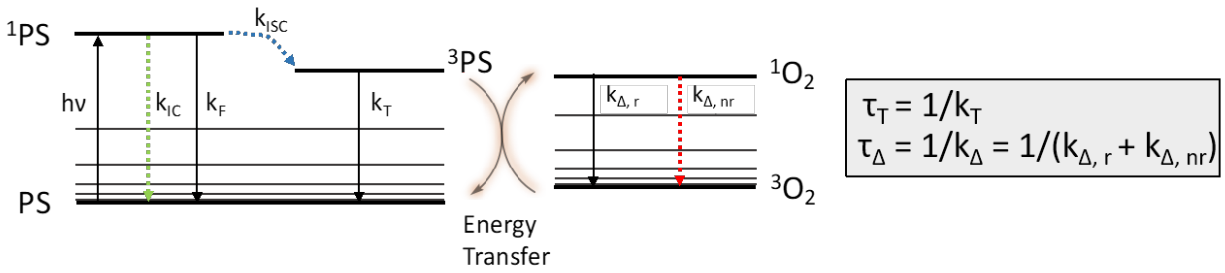

Scheme S2: Production of $^1O_2$ by a photosensitizer (PS), where hν represents an absorbed photon, k_{IC} is the internal conversion rate constant, k_{ISC} is the intersystem crossing rate constant, k_F is the fluorescence rate constant, k_T is the triplet PS rate constant, $k_{\Delta,r}$ is the radiative rate constant for $^1O_2$ deactivation, $k_{\Delta,nr}$ is the non-radiative rate constant for $^1O_2$ deactivation, τ_T is the triplet lifetime and τ_Δ is the $^1O_2$ lifetime.

According to scheme S2, the basic kinetic parameters that contribute to the $^1O_2$ production and decay are the ^{3}PS lifetime, τ_T, and the $^1O_2$ lifetime, τ_Δ. Therefore, the phosphorescence signal (S_t) of $^1O_2$ detected at 1275 nm presents a rise and decay bi-exponential behaviour, which can be modelled by the following expression.[19, 20]

$$S_t = S_0 \times \frac{\tau_\Delta}{\tau_\Delta - \tau_T} \times \left(e^{-t/\tau_\Delta} - e^{-t/\tau_T}\right) \qquad (S3)$$

This equation is valid for a PS in an homogenous environment. In heterogenous systems such a mesoporous nanoparticles, an additional decay component can be added in order to model adequately the experimental phosphorescence signals:[21]

$$S_t = S_{0,1} \times \frac{\tau_{\Delta 1}}{\tau_{\Delta 1} - \tau_T} \times e^{-\frac{t}{\tau_{\Delta 1}}} + S_{0,2} \times \frac{\tau_{\Delta 2}}{\tau_{\Delta 2} - \tau_T} \times e^{-\frac{t}{\tau_{\Delta 2}}} - \left(S_{0,1} \times \frac{\tau_{\Delta 1}}{\tau_{\Delta 1} - \tau_T} + S_{0,2} \times \frac{\tau_{\Delta 2}}{\tau_{\Delta 2} - \tau_T}\right) \times e^{-\frac{t}{\tau_T}} \qquad (S4)$$

The time-resolved near-infrared phosphorescence signals at 1275 nm for the three different PS@SiO_2 systems were collected in H_2O on the instrument described above. The signals and their fittings are presented in figure S25. As mentioned in the main manuscript, ERB@SiO_2 and RB@SiO_2 could be fitted with equation S4 presenting two components for $^1O_2$ lifetime decay (Table S3). On the other hand, the conventional bi-exponential equation (equation S3) modeled more adequately the experimental traces for BDP@SiO_2, providing a single lifetime τ_Δ for $^1O_2$.

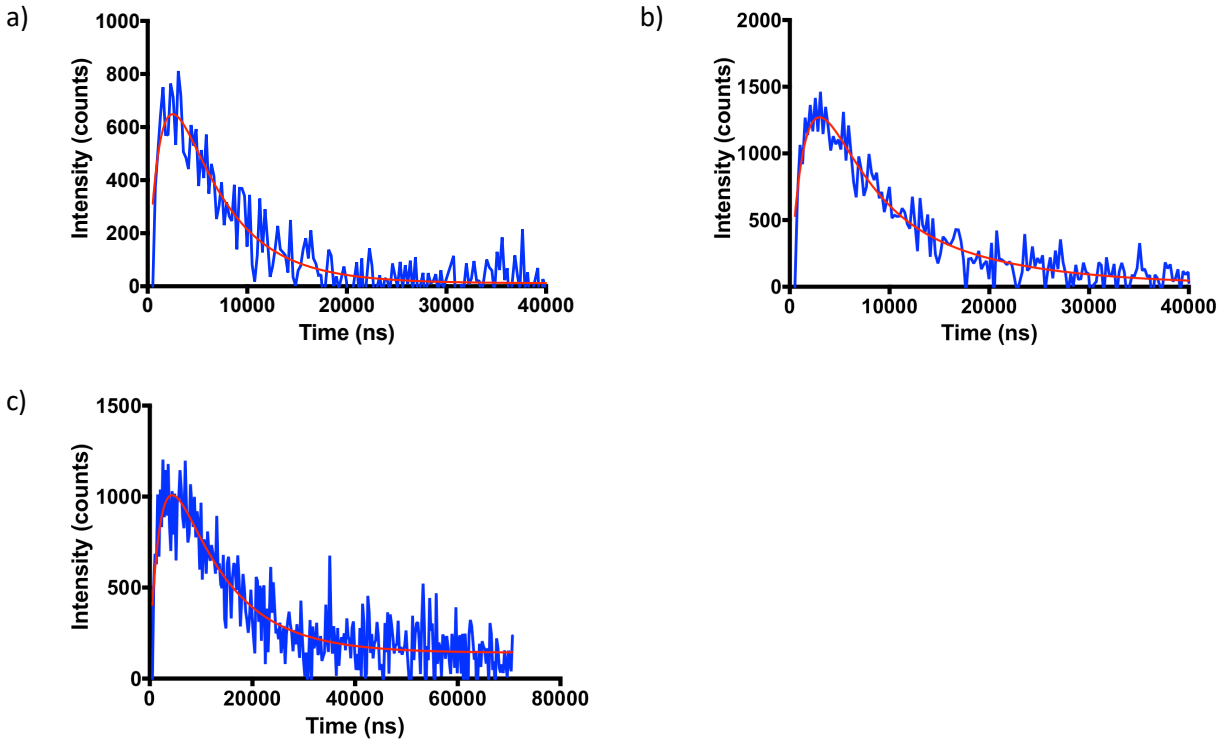

Figure S25: Time-resolved $^1O_2$ phosphorescence signals at 1275 nm and the corresponding fittings (red lines) for: ERB@SiO_2 – equation S4 (a); RB@SiO_2 - equation S4 (b); BDP@SiO_2 – equation S3.

Table S3: $^1O_2$ lifetime for the PS@SiO_2.

	τ_T (μs)	$S_{0,1}$ (a.u.) *RC (%)	$\tau_{\Delta 1}$ (μs)	$S_{0,2}$ (a.u.) *RC (%)	$\tau_{\Delta 2}$ (μs)
ERB@SiO_2	1.4	236 (22)	3.3	830 (78)	5.5
RB@SiO_2	1.8	1253 (56)	3.3	983 (44)	11
BDP@SiO_2	2.2	1310 (100)	11	-	-

*RC stands for the relative contribution, which can be estimated from the amplitude of the individual components $S_{0,1}$ (or $S_{0,2}$) related to the sum of all the contribution ($S_{0,1} + S_{0,2}$).

2.8. Indirect detection of singlet oxygen by an external probe.

Irradiation of samples was performed using a CW halogen lamp (300 W, 80 V) on a slide projector (Kodak) mounted with an appropriate cut-off filter. Thorlabs digital optical energy and power meter console PM100D, equipped with S121C photodiode power sensor was used to measure light power received by the sample. Samples were set up to receive 8.00 ± 0.02mW of light. To ensure selective photosensitizer irradiation, a 495 nm cut-off filter was used during the experiments (Figure S26).

Consider the following photochemical processes, with assigned rate constants, occurring in a solution containing a $^1O_2$ sensor, in our case 9,10-anthracenediyl-bis(methylene)dimalonic acid (ABDA), after excitation of a PS:

Light absorbance:	$^1PS + h\nu \rightarrow {}^1PS^*$	
Intersystem crossing:	$^1PS^* \rightarrow {}^3PS^*$	k_{ISC}
Energy transfer:	$^3O_2 + {}^3PS^* \rightarrow {}^1O_2 + {}^1PS$	k_{ET}
Singlet oxygen deactivation by the solvent:	$^1O_2 \rightarrow {}^3O_2$	k_Δ
Physical quenching by sensor (ABDA):	$^1O_2 + ABDA \rightarrow {}^3O_2 + ABDA$	k_p
Chemical interaction with sensor (ABDA):	$^1O_2 + ABDA \rightarrow ABDAO_2$	k_{ox}

We assume the direct reaction of PS in its ground state with the $^1O_2$ it produces is negligible. Under steady state approximation, i.e. no significant buildup of $^1O_2$ is expected, rate of the sensor disappearance can be written as the following, with Φ_{PS} representing the quantum yield of photosensitization, and I_{Abs} – the intensity of absorbed light:

$$\frac{d[ABDA]}{dt} = -k_{ox}[ABDA][{}^1O_2] = -k_{ox}[ABDA]\frac{\Phi_{PS}I_{Abs}}{(k_{ox}+k_p)[ABDA]+k_\Delta} \qquad (S5)$$

If the concentration of ABDA is small enough to assume that the term $(k_{ox}+k_p)[ABDA]$ is much smaller than the rate of singlet oxygen deactivation by the solvent (k_Δ), equation S5 can be simplified to:

$$\frac{d[ABDA]}{dt} = -k_{ox}[ABDA]\frac{\Phi_{PS}I_{Abs}}{k_\Delta} = -k_{PS}[ABDA] \qquad (S6)$$

The rate constant k_{PS} is simply a combination of a few constants. Therefore, the overall rate of ABDA degradation can be viewed as pseudo first order, or mathematically in the form of:

$$\ln[ABDA]_t = \ln[ABDA]_0 - k_{PS}t \qquad (S7)$$

By monitoring the sensor (ABDA) degradation, values of k_{PS} are determined experimentally for the various PS according to equation S7. In the experiments of free PS irradiation, concentrations of RB and ERB were 2 µM and 4 µM respectively. All PS@SiO_2 nanoparticles samples were prepared at 1 mg mL^{-1} nanoparticle concentrations. The concentration of the sensor probe was always 0.1 mM of ABDA. UV-Vis absorption

spectra were collected using a Varian Cary-50 single-beam spectrophotometer, results of the irradiation experiments performed in water and deuterium oxide, under inert nitrogen atmosphere and exposed to air are shown in figures S27-S29 in the main text.

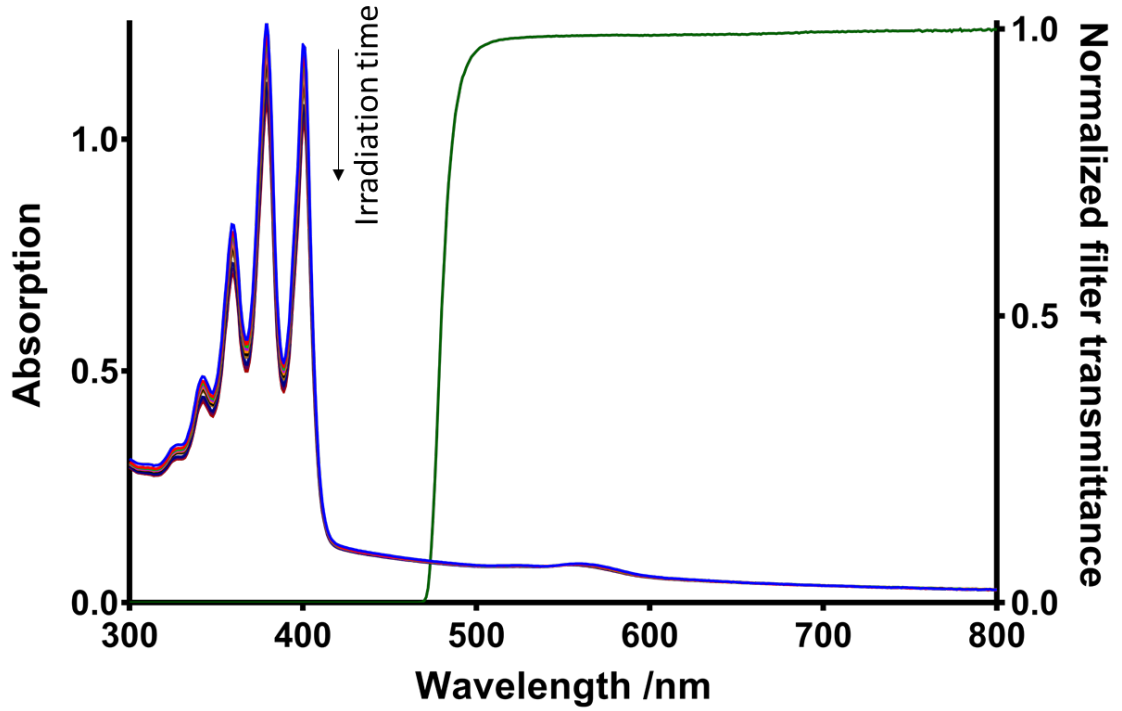

Figure S26: Sample raw data (left Y-axis) for the change of ABDA absorbance (monitored at 360 nm) due to the presence of RB@SiO_2 nanoparticles (with characteristic scattering and a peak at ~562 nm) upon irradiation. UV-Vis transmittance spectrum (right Y-axis) of the 495 nm cut off filter used to ensure selective PS irradiation is shown in green.

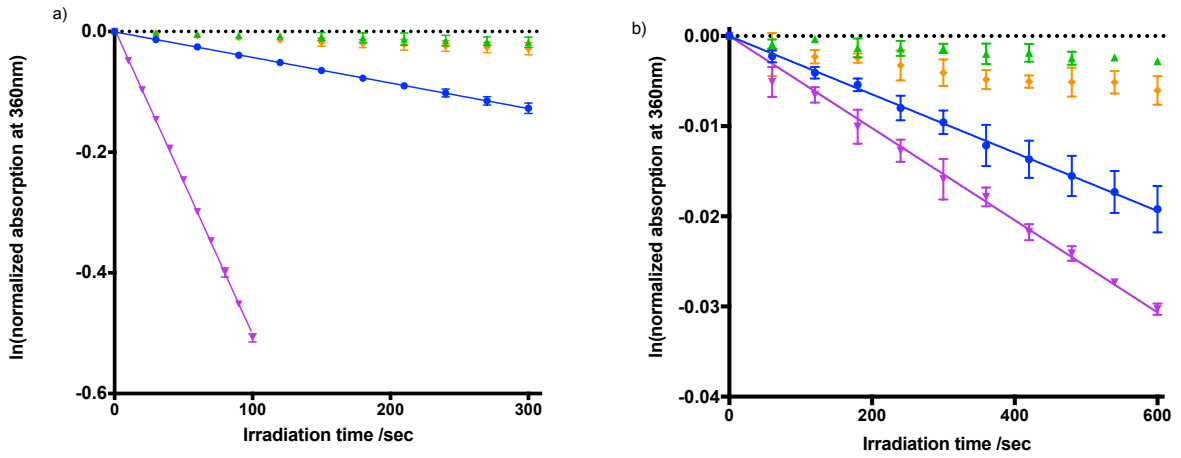

Figure S27: $^1O_2$ production kinetics data for the samples containing ERB free in solution (a); and ERB@SiO_2 nanoparticles (b). In both cases green triangles are for N_2 purged samples in H_2O; orange diamonds – N_2 purged samples in D_2O; blue circles – samples exposed to air in H_2O; purple inverted triangles – samples exposed to air in D_2O. $^{H2O}k_{PS}$ and $^{D2O}k_{PS}$ for ERB free in solution we found to be $4.23x10^{-4} \pm 0.02x10^{-4}$ s^{-1} and $5.06x10^{-3} \pm 0.03x10^{-3}$ s^{-1} respectively. $^{H2O}k_{PS}$ and $^{D2O}k_{PS}$ for ERB@SiO_2 we found to be $3.20x10^{-5} \pm 0.04x10^{-5}$ s^{-1} and $4.87x10^{-5} \pm 0.09x10^{-5}$ s^{-1} respectively.

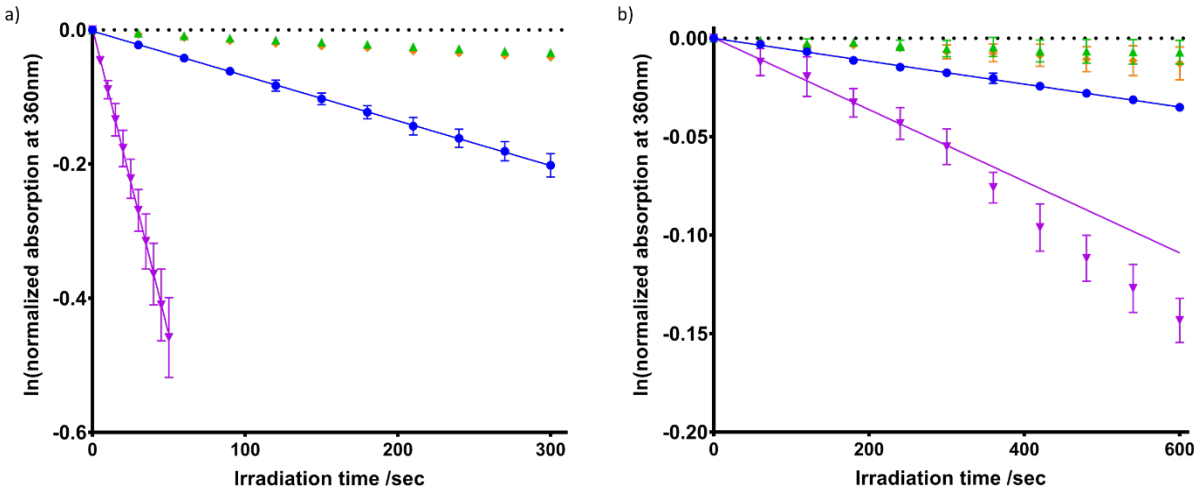

Figure S28: $^1O_2$ production kinetics data for the samples containing RB free in solution (a); and RB@SiO_2 nanoparticles (b). In both cases green triangles are for N_2 purged samples in H_2O; orange diamonds – N_2 purged samples in D_2O; blue circles – samples exposed to air in H_2O; purple inverted triangles – samples exposed to air in D_2O. $^{H2O}k_{PS}$ and $^{D2O}k_{PS}$ for RB free in solution we found to be $6.68x10^{-4} \pm 0.03x10^{-4}$ s^{-1} and $9.14x10^{-3} \pm 0.05x10^{-3}$ s^{-1} respectively. $^{H2O}k_{PS}$ and $^{D2O}k_{PS}$ for RB@SiO_2 we found to be $5.82x10^{-5} \pm 0.07x10^{-5}$ s^{-1} and $1.91x10^{-4} \pm 0.05x10^{-4}$ s^{-1} respectively.

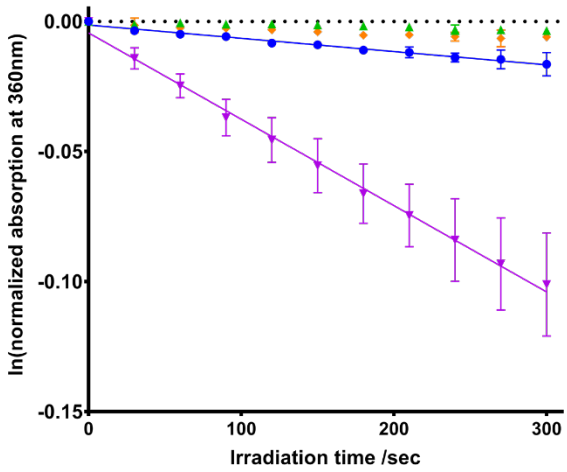

Figure S29: $^1O_2$ production kinetics data for the samples containing BDP@SiO_2 nanoparticles. In both cases green triangles are for N_2 purged samples in H_2O; orange diamonds – N_2 purged samples in D_2O; blue circles – samples exposed to air in H_2O; purple inverted triangles – samples exposed to air in D_2O. $^{H2O}k_{PS}$ and $^{D2O}k_{PS}$ for BDP@SiO_2 we found to be $5.1\times10^{-5} \pm 0.2\times10^{-5}$ s^{-1} and $3.32\times10^{-4} \pm 0.07\times10^{-4}$ s^{-1} respectively.

A summary of the data can be found in the table below.

Table S4. Assessment of singlet oxygen rate of production by PS systems† via indirect methodology using ABDA as a probe.

	$^{H2O}k_{PS}^{‡}/\ 10^{-4}\ s^{-1}$	$^{D2O}k_{PS}^{‡}/\ 10^{-4}\ s^{-1}$
ERB	4.23 ± 0.02	50.6 ± 0.3
RB	6.68 ± 0.03	91.4 ± 0.5
ERB@SIO2	0.320 ± 0.004	0.487 ± 0.009
RB@SIO2	0.582 ± 0.007	1.91 ± 0.5
BDP@SIO2	0.51 ± 0.02	3.332 ± 0.07

† All values reported are based on triplicate measurement with standard deviation given by ± value.

2.9. Fractions of singlet oxygen lifetime inside and outside of the nanoparticle.[22]

$^1O_2$ induced sensor (ABDA) degradation experiments were performed in H_2O and D_2O solvents. Since singlet oxygen spends part of its lifetime inside the silica nanoparticle and the other part in the solvent, overall singlet oxygen deactivation by the environment rate constant (k_Δ) can be written as:

$$in\ H_2O: \quad k_\Delta = g^{solvent} k_{H2O} + g^{SiO2} k_{SiO2} \qquad (S8)$$

$$in\ D_2O: \quad k_\Delta = g^{solvent} k_{D2O} + g^{SiO2} k_{SiO2} \qquad (S9)$$

Above, values of "*g*" are simply normalized weighing factors ($g^{solvent} + g^{SiO2} = 1$) which each represent the fraction of the lifetime that $^1O_2$ spends in the corresponding environment. Values of k_{H2O} and k_{D2O} are known from the literature to be 2.38×10^5 s^1, and 1.47×10^4 s^{-1},[23] while the values obtained by direct

detection of $^1O_2$ luminescence (in section 2.7) will be used for k_{SiO2}. The above equations can then be thought of as "2 equations with 2 unknowns" set, which can be easily solved by substituting equations S8 and S9 into equation S5:

$$\frac{d[ABDA]_{H2O}}{dt} = -k_{ox}[ABDA]\frac{\Phi_{PS}I_{Abs}}{(g^{solvent}k_{H2O} + g^{SiO2}k_{SiO2})} = {}^{H2O}k_{PS} \quad \text{(S10)}$$

$$\frac{d[ABDA]_{D2O}}{dt} = -k_{ox}[ABDA]\frac{\Phi_{PS}I_{Abs}}{(g^{solvent}k_{D2O} + g^{SiO2}k_{SiO2})} = {}^{D2O}k_{PS} \quad \text{(S11)}$$

By taking the ratio of the experimentally determined rates of ABDA degradation in the two solvents, values of $g^{solvent}$ and g^{SiO2} can be calculated by manipulating equation S12:

$$\frac{{}^{H2O}k_{PS}}{{}^{D2O}k_{PS}} = \frac{g^{solvent}k_{D2O} + g^{SiO2}k_{SiO2}}{g^{solvent}k_{H2O} + g^{SiO2}k_{SiO2}} \quad \text{(S12)}$$

3. References

1. H. E. Gottlieb, V. Kotlyar and A. Nudelman, *Journal of Organic Chemistry*, 1997, **62**, 7512-7515.
2. K. Krumova and G. Cosa, *Journal of the American Chemical Society*, 2010, **132**, 17560-17569.
3. X. Hong, Z. Wang, J. Yang, Q. Zheng, S. Zong, Y. Sheng, D. Zhu, C. Tang and Y. Cui, *Analyst*, 2012, **137**, 4140-4149.
4. P. P. Goswami, A. Syed, C. L. Beck, T. R. Albright, K. M. Mahoney, R. Unash, E. A. Smith and A. H. Winter, *Journal of the American Chemical Society*, 2015, **137**, 3783-3786.
5. S. Guo, H. Zhang, L. Huang, Z. Guo, G. Xiong and J. Zhao, *Chemical Communications*, 2013, **49**, 8689-8691.
6. V. R. Batistela, D. S. Pellosi, F. D. de Souza, W. F. da Costa, S. M. de Oliveira Santin, V. R. de Souza, W. Caetano, H. P. M. de Oliveira, I. S. Scarminio and N. Hioka, *Spectrochimica Acta Part A: Molecular and Biomolecular Spectroscopy*, 2011, **79**, 889-897.
7. N. C. Angeluzzi, M. Muñoz, D. T. Marquez, M. S. Baptista, A. M. Edwards, E. I. Alarcon and J. C. Scaiano, *Journal of Materials Chemistry B*, 2014, **2**, 4221-4225.
8. R. Boonsin, G. Chadeyron, J. P. Roblin, D. Boyer and R. Mahiou, *Journal of Materials Chemistry C*, 2016, **4**, 6562-6569.
9. S. T. G. Buck, F. Bettanin, E. Orestes, P. Homem-De-Mello, H. Imasato, R. B. Viana, J. R. Perussi and A. B. F. Da Silva, *Journal of Chemistry*, 2017, **2017**.
10. J. P. Pooler and D. P. Valenzeno, *Photochemistry and Photobiology*, 1979, **30**, 491-498.
11. B. Martins Estevao, F. Cucinotta, N. Hioka, M. Cossi, M. Argeri, G. Paul, L. Marchese and E. Gianotti, *Physical Chemistry Chemical Physics*, 2015, **17**, 26804-26812.
12. G. Alberto, I. Miletto, G. Viscardi, G. Caputo, L. Latterini, S. Coluccia and G. Martra, *The Journal of Physical Chemistry C*, 2009, **113**, 21048-21053.
13. B. Martins Estevão, F. Cucinotta, N. Hioka, M. Cossi, M. Argeri, G. Paul, L. Marchese and E. Gianotti, *Physical Chemistry Chemical Physics*, 2015, **17**, 26804-26812.
14. O. Valdes-Aguilera and D. C. Neckers, *Accounts of Chemical Research*, 1989, **22**, 171-177.
15. J. R. Lakowicz, *Principles of fluorescence spectroscopy*, Second edition. New York : Kluwer Academic/Plenum, [1999] ©1999, 1999.
16. X. Huang, N. P. Young and H. E. Townley, *Nanomaterials and Nanotechnology*, 2014, **4**.
17. M. Kruk, M. Jaroniec and A. Sayari, *Langmuir*, 1997, **13**, 6267-6273.
18. E. P. Barrett, L. G. Joyner and P. P. Halenda, *Journal of the American Chemical Society*, 1951, **73**, 373-380.
19. S. Nonell and S. E. Braslavsky, in *Methods in Enzymology*, Academic Press, 2000, vol. 319, pp. 37-49.
20. O. Planas, N. Macia, M. Agut, S. Nonell and B. Heyne, *Journal of the American Chemical Society*, 2016, **138**, 2762-2768.
21. G. Zampini, O. Planas, F. Marmottini, O. Gulias, M. Agut, S. Nonell and L. Latterini, *RSC Advances*, 2017, **7**, 14422-14429.
22. M. Hoebeke and X. Damoiseau, *Photochemical and Photobiological Sciences*, 2002, **1**, 283-287.
23. R. Schmidt and H. D. Brauer, *Journal of the American Chemical Society*, 1987, **109**, 6976-6981.